Experimental and Computational Approaches to Optimizing Bovine Gamete Cryopreservation

A Thesis Submitted to the
College of Graduate and Postdoctoral Studies
in Partial Fulfillment of the Requirements
for the degree of Master of Science
in the Department of Biology
University of Saskatchewan
Saskatoon

By
Frankie Tu

Permission to Use

In presenting this thesis in partial fulfilment of the requirements for a Postgraduate degree from the University of Saskatchewan, I agree that the Libraries of this University may make it freely available for inspection. I further agree that permission for copying of this thesis in any manner, in whole or in part, for scholarly purposes may be granted by the professor or professors who supervised my thesis work or, in their absence, by the Head of the Department or the Dean of the College in which my thesis work was done. It is understood that any copying or publication or use of this thesis or parts thereof for financial gain shall not be allowed without my written permission. It is also understood that due recognition shall be given to me and to the University of Saskatchewan in any scholarly use which may be made of any material in my thesis.

Requests for permission to copy or to make other use of material in this thesis in whole or part should be addressed to:

Head of the Department of Biology
Collaborative Science Research Building
University of Saskatchewan
112 Science Place
Saskatoon, Saskatchewan S7N 5E2 Canada

OR

Dean
College of Graduate and Postdoctoral Studies
University of Saskatchewan
116 Thorvaldson Building, 110 Science Place
Saskatoon, Saskatchewan S7N 5C9 Canada

Abstract

Cryopreservation uses freezing to suspend the metabolic activity of biological specimens for increased longevity of biotic materials like gametes. Cryopreservation has been known to affect both the functionality (performance of activities) and the viability (survival) of biological specimens during the freezing and thawing process due to four types of damage: (1) thermal, (2) ice, (3) osmotic stress, and (4) cytotoxic. Cryoprotective agents (CPAs) are known to reduce thermal and ice damage but cause osmotic stress and cytotoxic damage. Osmotic stress occurs when the addition of CPAs causes a rapid expulsion of water from the cell as the extracellular environment has become hypertonic. Cytotoxic damage occurs when a cell is exposed for too long to CPAs that may be damaging to the cell at high temperatures, but aid in preservation at low temperatures. The purpose of my project is to minimize osmotic stress in bovine embryos and cytotoxic damage in bovine sperm caused by CPAs using novel algorithmically guided techniques. To minimize osmotic stress in bovine embryos, I aim to facilitate the equilibration of embryos with cryoprotective agents isochorically (constant volume). Isochoric cryoprotectant equilibration, requires a feedback control system that in our case will use real-time image analysis developed in this thesis to estimate current embryo volume and then adjusts the concentration of CPAs being administered to the system. I implemented a colour-based image analysis software that was able to process images of bovine embryos as they were exposed to CPAs at a sub-second rate. The sub-second processing rates include cell volume estimates that are comparable to manual cell volume estimates. To minimize cytotoxic damage in bovine sperm, I optimized cryopreservation media (CPM) composition to maximize post-thaw motility. The composition of CPM can contain many ingredients that have the potential to interact and are infeasible to test only empirically. Here, I combined empirical experiments, data-driven optimization algorithms, and machine learning to optimize the composition of CPM. I used differential evolution and Gaussian process regression to optimize CPM composition that are on par with commercial media after 9 iterations. During the optimization process I determined that Gaussian process regression model was superior to artificial neural networks when predicting post-thaw motility for a given CPM composition. By optimizing these cryopreservation processes, cellular damage can be reduced, improving functionality and viability of gametes used in assisted reproductive technology that can be applied across animal husbandry and biomedical fields.

Acknowledgements

This project was funded by Semex USA, the National Sciences and Engineering Research Council of Canada, the National Institutes of Health, and the University of Saskatchewan.

I would like to thank my supervisor, Dr. James Benson for the support and guidance. Your assuredness and candid conversations helped me navigate the challenges in my project and gave me the confidence to direct my own research path. Furthermore, thank you for introducing me to interdisciplinary research and teaching me to communicate mathematics to an audience of biologists.

I also extend my gratitude to the experts on my committee, Dr. Chris Ambrose and Dr. Fangxiang Wu. Your input enriched and expanded my thesis as well as provoked thoughtful discussions about the applications of in silico analysis. Thank you to Joe and Robyn for sharing in the struggle of research and always being willing to lend an ear or a hand in my project. Furthermore, to Maajid, my deepest thank you for training me to be a laboratory biologist, for answering my endless questions, and for your mentorship throughout my project. My time in the lab would have been considerably more painful without your tutelage.

Finally, I want to express my profound gratitude to my incredibly insightful partner Jillian for your unwavering confidence in me throughout the journey and making me smile and laugh during the hardest times. You dealt with more then you deserved, especially during the writing phase. Your perspective on biological writing was integral to producing a thesis for an audience of math people, science people, and regular people. I look forward to a lifetime of London fogs and clever dialogue with you.

Contents

List of Tables

List of Figures

List of Abbreviations

ALSM	Approximated level-set method
ANN	Artifical neural network
CASA	computer-assisted sperm analysis
CPM	Cryopreservation media
CPA	Cryoprotective agent
DE	Differential evolution
DMSO	Dimethyl sulfoxide
GPR	Gaussian process regression
MSE	Mean Square Error
PBS	Phosphate-buffered solution
PID	Proportional-Integral-Derivative

1 General Introduction

1.1 Fundamentals of Cryobiology

Cryobiology examines the effect of low temperatures on biological systems [192]. The field of study ranges from understanding the adaptations of whole organisms in naturally occurring below-zero conditions (i.e., hibernation [17], cold hardiness [125], and use of anti-freeze proteins [55]) to developing techniques to preserve cells, tissues, gametes, or whole specimens [116, 192]. Arctic ground squirrels (Urocitellus parryii) are able to hibernate for weeks with a core body temperature that is below 0 °C [17]; these squirrels can survive subzero body temperatures by supercooling [17]. Supercooling is the process where a liquid is brought below the freezing point without ice formation, however, any extra energy input may cause ice nucleation. Plants can survive freezing temperatures depending on the their ability to acclimate to the cold. The cold acclimation process is initiated by exposure to low but non-freezing temperatures for an extended period of time [172]. During cold acclimation, physical and chemical changes affect the membrane [172, 179] and cryoprotectants in the form of sugars and proteins increase in the plant [6, 169, 172]. Through cold acclimation plants can survive between −5 °C to −30 °C, depending on the species [172]. As temperatures decrease so does the rate of biophysical processes (i.e., metabolic rates [41], chemical reactions, and diffusion [46]), until all biophysical processes cease [128, 201].

Cryopreservation, preservation via freezing, suspends the metabolic activity of biological samples and allows for decades of storage, long distance transportation, and fertility treatments [57, 201]. The general process of cryopreservation is as follows: cells are chilled to low temperatures (e.g. −80 °C) after the equilibration (when the movement of solution through the cell membrane is zero) of cryoprotective agents (CPAs) then the cells are plunged into liquid nitrogen for storage. Finally, cells are thawed (e.g. in a water bath at 37 °C or in the air) before use (e.g. post-thaw motility analysis or in-vitro fertilization) [140, 192]. Samples can be cryopreserved using "slow freezing" or "rapid freezing". In "slow freezing", samples are equilibrated with low concentrations of CPAs, and then slowly cooled down to anywhere between −40 °C to −80 °C. Then the samples are plunged into liquid nitrogen, an approach that reduces the probability of lethal intracellular ice formation [127]. In "rapid freezing", samples are equilibrated with a high CPA concentration and then plunged into liquid nitrogen to freeze the sample. Cryoprotective agents are additives used to preserve the viability and functionally during cryopreservation and thawing process [58]. Rapid freezing is the standard method for cryopreserving oocytes and embryos [9, 100, 116], while slow freezing is the standard method for cryopreserving sperm and many cultured cell lines [16, 68].

Cryopreservation of sperm has challenges not present with cell or tissue cryopreservation, due to their unique shape and function. There is inter- and intra- sperm variation and seasonal variations affect post-thaw motility and sperm quality [16, 114]. Sperm cryopreservation requires multiple media components to preserve mechanical functionality (ability to swim) [10, 24, 33, 180]. Some common additives are egg yolk which is used as a membrane stabilizer [137], fructose is used as an energy source [132], and glycerol as the permeating CPA used during cryopreservation. Many other additives (e.g. 3-O-methylglucose [27], glutathione [197], trehalose [202]) have been investigated to improve post-thaw functionality and viability.

Cryopreservation induced cell death can be split into cell lysis, apoptosis, or necrosis. Cell lysis is when cell membrane is abruptly compromised either by ice or osmotic response. Intracellular ice formation can damage the cell membrane and during the cryopreservation process the cells volume can fluctuate beyond its biophysical limit [18]. Apoptosis is programmed cell death caused by environmental and developmental factors [28]. When apoptosis is initiated the cell ceases function by breaking down its structural components and small cell fragments break away from the dying cell. For instance, cryopreservation can damage the DNA in sperm [45] which does not impact fertility, however, embryos that were fertilized with DNA damaged sperm can induce apoptosis [52]. Necrosis is pathological cell death caused by sudden and extreme trauma (e.g. cell exposed to cytotoxic CPA [18, 97]) which results in death. Once the necrosis process has started the cell swells until it ruptures and the intercellular constituents are released into the extracellular medium.

1.2 Assisted Reproductive Technology

Assisted reproductive technologies are the techniques used to improve or control fertility. Some procedures include artificial insemination, in vitro fertilization, and cryopreservation of sperm, oocytes, and embryos. Artificial insemination is the delivery of sperm directly into the cervix to increase the sperm density at the fertilization site [136]. The first successful artificial insemination in a dog was done by Lazzaro Spallanzani in 1784 [19, 136, 203]. The first documented artificial insemination of humans was by John Hunter in 1770 [136]. With in vitro fertilization the sperm and oocyte are incubated together for a period of time. In 1959, Chang [32] was the first to successfully fertilize rabbit ova in vitro. The first human baby as a result of in vitro fertilization was in 1978 [89, 168].

Cryopreservation has allowed for the genetics of elite animals to be be distributed internationally [96, 192]. In 1949, Polge et al. [144] discovered glycerol as a cryoprotectant and allowed for the successful cryopreservation of sperm, which subsequently increased the use of artificial inseminations in the dairy and beef industry [70]. The International Embryo Technology society reported that in 2018, industry created 1.5 million embryos worldwide and 69% of those embryos were cattle [184]. Cryopreserved embryos enhance the genetic selection process in the cattle industry while cryopreserved sperm is widely used in artificial insemination and in vitro fertilization [139, 192]. Artificial insemination and in vitro fertilization allow for strategic herd management in domestic animals, as producers may select for genetic traits that maximize

profitability [96, 115]. For instance, milk production has increased significantly between 1960 to 2010 [74, 96]. In beef cattle, being able to predict the breeding value of a sire may increase the rate of genetic change [26, 96] which subsequently could lead to increased profitability [75, 96]. Furthermore, cryopreserved gametes can be used for conservation purposes and genetic or even reproductive material from postmortem animals may still be viable [20].

1.3 Issues in Reproductive Cryopreservation

The ultimate goal of cryopreservation is to freeze and thaw biological specimens while preserving both functionality and viability [116, 192]. Functionality simply refers to a specimen's ability to perform activities after freezing at a level that is comparable to before freezing, while viability is a measure of post-thaw survival. A measure of viability is cell membrane integrity [180]. For embryos, functionality is measured via successful pregnancy and delivery of a live offspring [100]. Currently, cryopreserved human embryos result in a delivery rate of between 17.7% and 24.8%, while fresh embryo delivery rate is 27.8% [100]. Viability rates for cryopreserved bovine embryos range from 36.9% to 39.4% [11]. In sperm, functionality is measured through motility of the sperm as motility directly correlates with fertilization rates [33, 60, 72, 108, 166]. Sperm with low motility are less likely to reach the fertilization site and fertilize an oocyte in vivo [14, 68]. Non-frozen sperm are estimated to have a 50% motility rate, while post-thaw sperm have a reduced rate of 30% [77]. In terms of viability, $40 - 50\%$ of sperm do not survive the freeze-thaw cycle [68, 79, 189]. The decrease in both functionality and viability for embryos and sperm after cryopreservation affirms that the cryopreservation process is damaging to biological specimens. Currently, there are four main cryopreservation induced factors that are known to contribute to the decrease in functionality and viability: (1) thermal damage, (2) formation of ice crystals within the cell, (3) osmotic stress, and (4) cytotoxicity [39, 71, 92]. Each of these will be discussed below.

Thermal damage occurs when a specimen is cooled to temperatures above 0 °C [15, 54, 145]. For oocytes, thermal damage disrupts the cell membrane, the cytoskeleton, and cortical granules [4, 143, 185, 192]. Disruptions to the cortical granules and cell membrane decrease fertilization of oocytes [65, 185, 192]. For bovine embryos, they appear morphologically normal immediately after cooling, but once returned to normothermic temperatures, the cell membrane can disintegrate [15]. Occurrences of thermal damage is dependent on species, developmental stage, and whether embryos were developed in vitro or in vivo [15, 99, 145]. Thermal damage disrupts the cell membrane of sperm during cooling [54] which is known to decrease fertilization rates in post-thaw sperm [14, 68, 138].

While thermal damage occurs at temperatures above 0 °C, ice formation becomes a considerable factor of cell damage at subzero temperatures. Ice formation can occur in both the extracellular and intracellular space. During the freezing and thawing cycle, passing through the −15 °C to −60 °C range has the greatest potential for damage as this is the point for extracellular ice formation [122, 138]. Ice formation occurs in the

extracellular solution when a seed or nucleation point provides a location for ice crystals to nucleate [59, 193]. As ice formation increases, the ice may begin to form on the cell membrane. While the cell membrane initially prevents extracellular ice from entering the cell [120, 138], intracellular ice formation begins at locations along the cell membrane that have seeded extracellular ice formation [104]. Intracellular ice formation may damage the cell membrane leaving the cell osmotically inactive [43, 123, 138] and ultimately result in loss of viability of cells following post-thaw.

Osmotic stress is caused when the osmolarity of extracellular environment causes volume to change by water loss or by water gain. For instance, osmotic stress can be caused by a hypertonic extracellular environment. Osmotic stress can result in damage to the cell membrane [101, 127] and affects cell viability post-thaw [133, 200]. At temperatures below 0 °C, when water turns into ice, the salt concentration increases in the remaining unfrozen solution, resulting in a hypertonic extracellular solution and expulsion of water from the cell [190]. This sudden change in solute concentration, and corresponding loss of water increases osmotic stress [190].

To protect cells against thermal, ice, and osmotic damage, cryoprotective agents (CPAs) are added to the freezing process [54, 138]. Cryoprotective agents include both permeating and non-permeating forms that serve various purposes. Permeating and non-permeating CPAs reduce relative ion concentration during the freezing process, limiting osmotic stress [45, 59, 109]. Permeating CPAs pass through the cell membrane and replace intracellular water, limiting ion concentrations as well as intracellular ice formation during freezing [116, 154]. In sperm, permeating CPAs help stabilize the cell membrane and preserve intracellular structure [54, 98, 165]. During the thawing process, non-permeating CPAs also prevent excessive cellular swelling [192].

While CPAs are helpful in preventing thermal, ice, and osmotic damage, they also contribute to cell damage. When CPAs are added to the extracellular environment, the environment becomes hypertonic, resulting in a large and rapid decrease in water volume within the cell (osmotic stress) [59, 165]. After this initial expulsion of water, CPA diffuses into the cell until CPA equilibration occurs (the point where solute concentration is the same both inside and outside the cell). Osmotic tolerance limits dictate a region where cells may shrink and swell osmotically with little or no damage [23, 63], but the addition of CPAs may require a cell to respond beyond its osmotic tolerance limits.

Further to osmotic stress, CPAs also present an additional challenge to cell functionality and viability as CPAs are cytotoxic [88, 140]. Cryoprotective agent toxicity may kill cells in the order of seconds to minutes depending on the concentration [39, 47, 50, 188]. The cytotoxic effects of CPAs include damage to the cell membrane, impairment of cell and embryo development, reduced sperm motility, and damage to other macromolecules [25, 141]. To alleviate cytotoxic effects of CPAs, a combination of different CPAs can be used [192]. For a biological sample to be successfully cryopreserved an optimal balance of CPAs is required.

Along with the cryopreservation factors that contribute to reduced viability and functionality, different cell types also present their own challenges. For example, oocytes have a small surface area to volume ratio, they are more sensitive to cryopreservation injury [8, 156, 161, 176, 199] and the zona pelucida impedes

water movement which increases the likelihood of intracellular ice formation [161]. Sperm cryopreservation is a complex procedure that requires cryopreservation media containing both permeating and non permeating CPAs and whist cellular damage is being accumulated at every step [27, 150, 165].

1.4 Reproductive Cryobiology In Silico

Mathematical models have been developed to predict optimal cryopreservation conditions. For example, a two-parameter solute solvent transport model [62, 130] was developed from work done by Jacobs and Stewart [86] and Jacobs [85]. Over the years other models have been developed to understand water and CPA transport by Kedem and Katchalsky [91] and Mazur [119, 121]. These models relate cell membrane permeability [86, 91, 119], cell volume [86, 91, 119], and the transition of extracellular to intracellular ice [119]. Mullen et al. [130] used the two parameter model to determine the optimal CPA concentration, CPA composition, and multistep CPA equilibration process in bovine oocytes. Recently, models have been developed by Davidson et al. [40] and Benson et al. [23] to optimize the cryopreservation process such that damage due to CPA toxicity were minimized. However, these models require estimates or measurements of parameters including cell membrane permeability to water and CPA, the surface area of the cell, among others before they can be used.

Some model parameters can be estimated by observing the volume response of cells in anisomotic conditions. To estimate some model parameters, one possibility is to use image analysis to get cell membrane permeability and surface area parameters, a first step is to estimate cell volume from images captured during CPA equilibration. Manual (e.g. hand drawn) volume estimates is the standard approach [76, 105, 130, 153]. A number of samples are required in order to produce accurate estimates [51, 105, 130] due to cell to cell variability [129, 181]. However, manual volume estimates are time intensive and prone to error [162, 167]. Recently, automated cell volume estimation tools have been developed for use [107, 124, 167]. For instance, Mbogba et al. [124] trained, validated, and tested a machine learning approach to cell volume estimation. Machine learning is a set of algorithms that allows for a computer to learn a set of rules or a model from a dataset [7, 67]. A machine learning approach is immensely time consuming, as machine learning algorithms need time to be trained and tested and the data used for this is created manually [124]. These automated approaches have only been applied post-experiment which saves manual labour time. However, the possibility of doing automated cell volume estimates live during the experiment has yet to be explored, most likely due to typically long image processing times [107, 167].

1.5 Thesis Objectives

In order to increase functionality and viability of both embryos and sperm, understanding how the cryopreservation process influences the biophysical properties of bovine oocytes, embryos, and sperm is essential. I used novel machine learning and mathematical models to optimize cryopreservation techniques. Given the

complexity of factors that contribute to reductions in cell functionality and viability after cryopreservation, I focused on the effect of CPAs through (1) osmotic stress and (2) cytotoxicity.

(1) For osmotic stress, I built tools to enable the optimization of the equilibration of CPAs such that the process is isochoric (constant volume) for bovine oocytes and embryos in order to reduce the effect of osmotic stress. I used numerical analysis techniques and physical manipulation of fluid delivery systems to monitor and respond to cell volume changes of oocytes and embryos during CPA addition. The techniques were developed to respond to each tissue that underwent CPA equilibration to achieve optimized isochoric CPA equilibration at an individual level.

(2) For cytotoxicity, I optimized the composition of cryopreservation media (CPM; including CPAs) added to the cryopreservation protocol of bovine sperm in order to reduce cytotoxicity and maximize post-thaw motility. I used novel machine learning and mathematical algorithms to enhance previous approaches to optimize freezing media composition. This approach not only optimized the media components, but also created a new method for optimization of media composition.

1.6 Structure of Thesis

My thesis is separated into four chapters. **Chapter 1: General Introduction** (above) covers information that illustrates the details of my thesis objectives. **Chapter 2: Volumetric Optimization of Oocytes and Embryos** seeks to provide evidence that isochoric equilibration is possible for individual cells and tissues through novel cryopreservation techniques to decrease osmotic stress. The results of this chapter compare the precision of technology-determined and manual estimates of volume estimates, and underscores the necessity of real-time volume estimation for CPA equilibration. **Chapter 3: Optimization of Media for Sperm Cryopreservation** explores the application of a data driven approach to improve cryopreservation media formulas above the industry standard. Specifically, this chapter uses machine learning algorithms to address the nuanced media requirements needed for improved post-thaw performance in motile cells like sperm. **Chapter 4: General Discussion** provides a synthesis of both data chapters and explores the future directions and applications of this research.

2 Volumetric Optimization of Oocytes and Embryos

2.1 Introduction

Oocytes and embryos are reproductive cells and tissues that are frequently isolated for cryopreservation. Cryopreservation of oocytes and embryos has enabled herd management in agriculture systems [84, 116] and assisted reproduction treatments in humans [62, 130]. The current method for cryopreserving oocytes and embryos requires them to be equilibrated (when the movement of solution through the cell membrane is zero) with high concentrations of cryoprotective agents (CPA) [62, 147, 161]. Cryoprotective agents stabilize the cell's membrane, decrease water in the cell to reduce the risk of intracellular and extracellular ice formation, and reduce the relative concentration of ions [49, 118, 137]. However, as discussed in Chapter 1, CPA addition is associated with osmotic stress and cytotoxicity, which must be balanced to optimize cryopreservation outcomes.

When cells are exposed to high CPA concentrations, the cell can shrink or swell past volume limits, known as osmotic tolerance limits [101]. Thus, the osmotic response to CPA is mechanically stressful and can cause damage to the cell membrane [101, 191]. This osmotic stress can affect post-thaw fertility [3]. For example, Agca et al. [3] showed that bovine oocytes exposed to high osmolarities causes a significant osmotic response which reduces in vitro blastocyst development by roughly 50% when compared to control cells in isotonic solution. Therefore, the CPA equilibration process must consider the osmotic response of the cell.

At least two potentially optimal methods have been proposed to optimize CPA equilibration: (1) time optimal and (2) toxicity optimal [23, 40, 90]. The time optimal protocol loads as much CPA into a cell as fast as possible reducing a cell's exposure time to CPA and its cytotoxicity. This time optimal approach causes an osmotic response in the cell where it shrinks to its lower osmotic tolerance limit due to high concentrations of CPA outside the cell [21, 40]. The toxicity optimal protocol minimizes the cytotoxic effects of CPA during the loading phase by slowly exposing a cell to CPA over a longer period of time. The toxicity optimal protocol causes the cell to swell to its upper osmotic tolerance limit as the low concentration of CPA causes a hypotonic environment [39]. As both of these methods require the cell to reach its osmotic tolerance limits, the cell undergoes increased osmotic stress.

Due to the increased osmotic stress of the current optimization protocols that focus on cytotoxcity, a more optimal approach could balance cytotoxicity and osmotic stress together. To minimize osmotic stress, it is common to use a multistep method for adding or removing CPA until equilibration is reached [23, 187]. The incremental increase of CPA concentration lowers the osmotic stress [64, 102] by limiting excessive volume

changes in the cell which is known as the volumetric optimal approach [101]. Levin and Miller [102] and Levin [101] demonstrated this theoretically that by actively controlling both permeating and nonpermeating solute concentrations in the extracellular media, an isochoric (constant volume) CPA equilibration approach could be achieved. They proposed that the changes to extracellular CPA concentrations should induce an exchange of water volume and permeating CPA volume in a 1:1 ratio for a single isolated cell, such that osmotic stress is reduced and a constant volume is maintained [102]. By equilibrating oocytes and embryos using the volumetric optimal approach, the functionality and viability of post-thaw tissues may improve.

Previously, it has been theorized that this volumetric optimal, or isochoric, approach could be applied empirically [101]; however, the difficulties of predicting extracellular CPA concentrations as a function of cell volume have restricted the implementation. Moreover, the concentration dependence of membrane permeabilities is not understood for more then a handful of cells [94]. Finally, there is cell to cell variation in osmotic response [95]. Therefore, both precise control of extracellular CPA concentrations and real-time volume estimation are required. Microfluidic devices allow for precise control of extracellular CPA concentrations [76, 106].

Microfluidic devices handle and analyze fluids at a micrometer scale [78], allowing for more acute control of solution tonicity and accurate modeling of the cell's osmotic response [106]. These devices have been used in cryopreservation in the past. For example, Heo et al. [76] used a microfluidic device that equilibrated cells with CPA such that the volume change was $< 10\%$ over 10 minutes. Their study was able to control extracellular CPA concentration, but it was not formally coupled with the response in cell volume.

Real-time estimates of cell volume during CPA equilibration creates a baseline volume estimate of the cell before equilibration begins as well as records volume changes as CPA is introduced to the system. These estimates can then be used to adjust CPA concentrations to restrict volume changes. These estimates are calculated from images captured during the CPA equilibration process.

Implementation of this approach is challenging. To wit, manual and machine learning volume estimates are time intensive and prone to error [124, 153, 167]. For example, the model by Sadanandan et al. [159] took 6 seconds to process a single image. While one image is being processed, CPA continues to be added at a rate that induces an osmotic response in a hypertonic/hypotonic environment resulting in osmotic stress. Therefore, the possibility of successful feedback control of CPA equilibration is reduced. In contrast, active contour methods can be used for real-time image analysis, which is essential for volumetric optimization of CPA equilibration and avoids osmotic stress. The level-set method is a simple and flexible active contour method [103, 195] that segments an image (separates the foreground from the background) by expanding or contracting a level-set. A level-set simply defines a boundary within a contour plot or image that has the same pixel intensity value (Figure 2.1).

The level-set method has been successfully used to segment the corpus luteum in bovine ovarian ultrasound images to within 1-2 mm [157]. Furthermore, it has been effective in segmenting objects in real-time as their location changes in the image [69, 164, 171]. Gulyanon et al. [69] showed that objects can continue to be

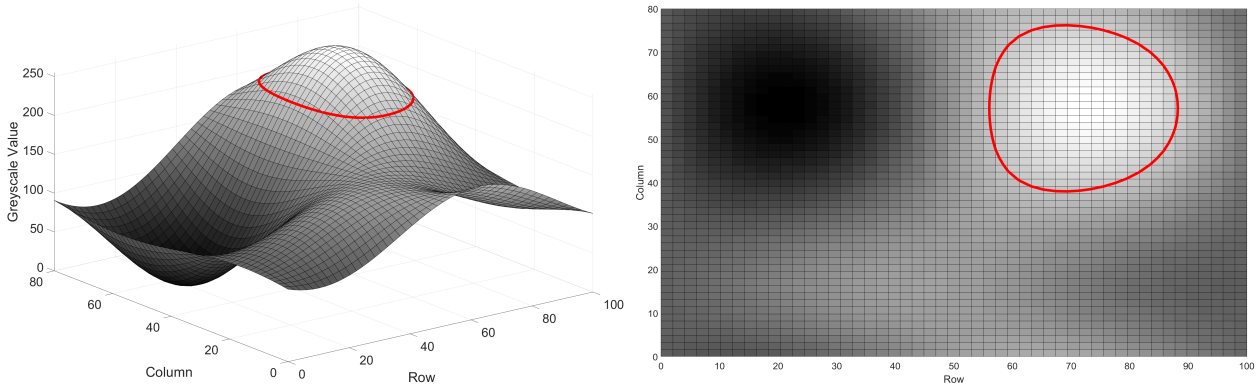

(a) **(b)**

Figure 2.1: Level-set segmentation draws contour line(s) around all the pixels with a given greyscale value. Figure 2.1a shows greyscale values of Figure 2.1b on the vertical axis and a contour has been drawn around all pixels with a greyscale value of 200. The user sees Figure 2.1b with the contour line separating foreground pixels (inside the contour) from background (outside contour).

segmented after an obstruction of view occurred. The flexibility of the level-set method could allow for improved and speedy image analysis and volume estimation in oocytes and embryos which may facilitate the development of a volumetric optimal approach.

2.1.1 Objectives

The purpose of this study was to use experimental and computational techniques to minimize osmotic stress in bovine oocytes and embryos during CPA equilibration using the volumetric optimal approach. This approach may balance the osmotic tolerance consequences of the time- and toxicity optimal approaches [22, 40, 90, 111] to improve post-thaw functionality and viability of bovine reproductive tissues. I had two central objectives: (1) to design a microfluidic device to provide controlled flow of CPA and (2) to modify standard image analysis techniques for implementation in real-time to estimate cell volume.

2.2 Methods

2.2.1 Bovine Oocytes and Embryos

Ovaries from domestic cattle were sourced from an abattoir. The ovaries were transported to Semex (Quebec, Canada) in warm ($36 - 38$ °C) phosphate-buffered solution (PBS) in a thermos flask within 3 hours of culling. Technicians at Semex extracted ovarian follicles ($3 - 8$ mm in diameter) with a 19-gauge needle and placed them under a microscope with a 20x objective lens. They selected cumulus-oocyte-complexes in tertiary stage follicles (Figure 2.2a) to be cultured to the mature oocyte stage. They washed the cumulus-oocyte-complexes twice and cultured them in groups of $20 - 30$ for $18 - 22$ hours at 38.5 °C. The culture medium contained HEPES modified tissue culture medium 199 supplemented with 10% FBS, 10 IU/mL pregnant mare serum

gonadotrophin , 5 IU/mL human chorionic gonadotrophin (PG600, Intervet, Milton Keynes, UK), 0.2 mM pyruvate, and antibiotics. Some oocytes had cumulus cells removed mechanically using a $122 - 124$ μm denuding pipette (Vitrolife) and were shipped to the University of Saskatchewan in an incubator (MicroQ) maintained at 38.5 °C. Other oocytes underwent in-vitro fertilization to become embryos. The fertilized ova were incubated for 18 hours. The early zygotes were washed and placed in embryo development medium. On Day 4, the embryos in early morula stage (Figure 2.2b) were placed in a 15 mL tube and shipped to University of Saskatchewan in the same method as for oocytes. Upon arrival, I washed the oocytes and embryos with Oocyte Wash medium (Boviteq) in preparation for trials using the image analysis software.

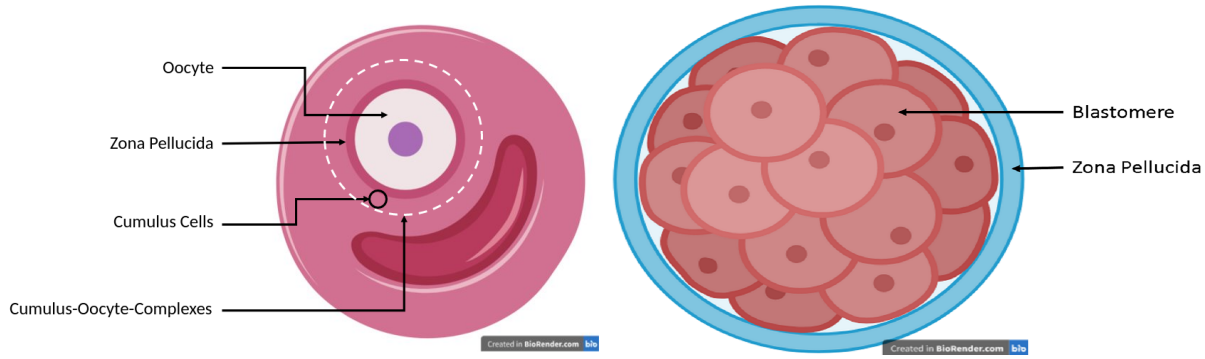

Figure 2.2: A tertiary stage follicle (a) with the cumulus-oocyte-complex circled in white and a day 4 morula embryo (b).

2.2.2 Microfluidic Device

I created a microfluidic device (Figure 2.3) to maintain isochoric conditions for oocytes and embryos during CPA equilibration. I designed the microfluidic device in SketchUp 2017 and used 3D printing (MakerBot Replicator 2X) to generate prototypes and the final design. Solutions A, B, and O (outlet) were connected to individual syringe pumps, and the flow rates (R) $R_{\mathrm{A}} + R_{\mathrm{B}} + R_{\mathrm{O}} = 0$. To capture the osmotic response in embryos, I filled syringe A with saline (0.35x PBS) and syringe B with CPA (30% DMSO in 0.35x PBS). The prepared embryo was suspended in 1X PBS and held with a glass pipette tip (Sunlight Medical) via vacuum in the viewing stage of the device. The small volume of the viewing stage enabled the entire system to equilibrate to new CPA concentrations in approximately $t = V_{\mathrm{total}}/(R_{\mathrm{A}} + R_{\mathrm{B}})$ seconds, where V_{total} is the volume of the channel leading to the viewing stage. As solution A and B were perfused into the viewing stage, I captured and analyzed the embryo's osmotic response using my image capture software (2.2.3).

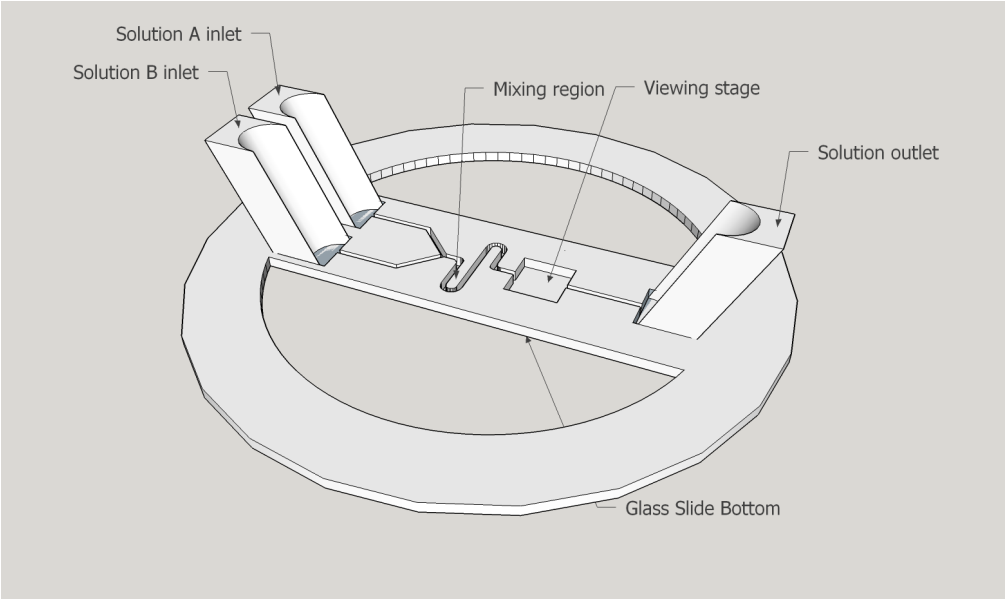

Figure 2.3: Microfluidic device designed in SketchUp 2017 has two inputs and one output. Solutions pass through a mixing region before entering the viewing stage where an oocyte or embryo is held with a glass pipette tip. The bottom of the device has a glass slide attached while the top is exposed.

2.2.3 Microscopy and Image Capture Software

I used a Nikon Eclipse TE-3000 Inverted Florescence Microscope with 40x objective lens to capture phase contrast and bright field images of the oocytes and embryos. I mounted a Motic 2 Megapixel camera to the microscope for image collection. Motic provides proprietary imaging software that records video and captures images at predefined intervals for post-trial analysis. However, as I performed real-time image analysis of cellular response to CPA addition, I created image capture software that was concurrent with the trial. I used the software development kit provided by Motic which includes functions that communicate directly with the camera. The software captures high-resolution (1600×1200) colour images up to 10 frames/second allowing for real-time image analysis.

2.2.4 Image Analysis Software

I built image analysis software to estimate the volume of the oocytes and embryos following the addition of CPA. I executed the image analysis software on two computers (Table 2.1).

Table 2.1: Specifications for computers used for image analysis.

	Computer 1	Computer 2
OS	Pop OS 20.04 LTS	Raspberry Pi OS
CPU	Intel Core™ i7-8750H	Broadcom BCM 2711
RAM (GB)	16	4
GPU	NVIDIA Quadro P1000 Mobile	NA

Preliminary trials using other image segmentation methods yielded subpar segmentation results for bovine oocytes. Initial image segmentation attempts using adaptive thresholding and watershed methods were applied to grayscale bovine oocyte images. These segmentation methods yielded subpar results, as thresholding captured the oocyte along with a majority of the background and watershed captured could not distinguish the oocyte boundary due to low contrast between the boundary and background. The active contour approach built into MATLAB (Version 2019a, Mathworks, USA) showed the most promising results at the beginning of the dataset. However, the contour eventually drifted away from boundary causing segmentation accuracy to rapidly decrease. Thus, I decided to use the level-set method, a type of active contour approach, based on the performance of the Matlab algorithm, its simplicity, and ease at which it can be generalized to segment multiple samples simultaneously.

I used an approximated level-set method (ALSM) to define the edge of the oocyte or embryo from which the volume can be determined. I implemented ALSM with two different speed functions: (1) grayscale [164] and (2) colour-based [183]. Both approaches are based on the algorithm (Algorithm 1) in Shi and Karl [164].

Algorithm 1 The general structure of the ALSM algorithm based on Shi and Karl [164].

```
compute F̂
while (stop_condition() == False) or (current_iteration < max_iteration) do
    switch_in()
    remove_redundant_in()
    switch_out()
    remove_redundant_out()
end while
```

First, the algorithm computed $\widehat{F}$. $\widehat{F}$ is an approximated speed function that defined all the edges in the image by calculating relative change in intensity between pixels. I used an approximated speed function because traditional level-set required solving a partial differential equation which is computationally expensive and not feasible for real-time image analysis of high-resolution colour images.

For the grayscale ALSM, I created a prototype in MATLAB (Version R2019a, Mathworks,USA) using test images of immature primate follicles before implementation on bovine oocytes. I debugged and verified the prototype, then I reimplemented the software in C/C++ for speed, portability, and linkage with the

image capture software.

For the colour-based ALSM, I used a colour tensor (matrix of partial derivatives of the image) outlined by Van de Weijer and Gevers [183]. Let A be the colour tensor

$$A = \begin{bmatrix} I_x^T I_x & I_x^T I_y \\ I_y^T I_x & I_y^T I_x \end{bmatrix}, \tag{2.1}$$

where I is the colour image and I_x and I_y represents the partial derivative of image with respect to the horizontal (x) or vertical (y) direction. In a colour image (I), three channels that represent the primary colours (red (R), green (G), and blue (B)) are combined to produce all colours in electronic images. I substituted the R, G, and B channels of I into A, where the colour tensor became

$$A = \begin{bmatrix} R_x^2 + G_x^2 + B_x^2 & R_x R_y + G_x G_y + B_x B_y \\ R_x R_y + G_x G_y + B_x B_y & R_y^2 + G_y^2 + B_y^2 \end{bmatrix}. \tag{2.2}$$

I then defined the eigenvalues from this colour tensor

$$\lambda_1 = \frac{1}{2}\left(I_x^T I_x + I_y^T I_y + \sqrt{\left(I_x^T I_x - I_y^T I_y\right)^2 + \left(2 I_x^T I_y\right)^2} \right), \tag{2.3}$$

$$\lambda_2 = \frac{1}{2}\left(I_x^T I_x + I_y^T I_y - \sqrt{\left(I_x^T I_x - I_y^T I_y\right)^2 + \left(2 I_x^T I_y\right)^2} \right), \tag{2.4}$$

where $\lambda_1 + \lambda_2$ corresponds to total local derivative energy [183]. The new approximated speed function became

$$\widehat{F} = \sqrt{\frac{\lambda_1 + \lambda_2}{\max(\lambda_1 + \lambda_2)}}, \tag{2.5}$$

where $\max(\lambda_1 + \lambda_2)$ is the maximum intensity of colour shift between pixels and the square root is based on the Prewitt edge detection algorithm [148].

Because $\widehat{F}$ defines all edge features of an image, there are extraneous edges found in the images of oocytes. For example, not only is the cell boundary defined, but intracellular organelles are defined as well. I defined an initial boundary for the level-set in a small region around the oocyte. I then initiated functions (Algorithm 2 - Algorithm 5) to define the actual boundary by adding and removing pixels one at a time based on their criteria.

I let $\widehat{\phi} = \widehat{\phi}(x)$ denote the approximated level-set with integer values $\{3, 1, -1, -3\}$ as follows

$$\widehat{\phi}(x) = \begin{cases} 3, & \text{if } x \text{ is a background pixel} \\ 1, & \text{if } x \in L_{\text{out}} \\ -1, & \text{if } x \in L_{\text{in}} \\ -3, & \text{if } x \text{ is a foreground pixel} \end{cases} \tag{2.6}$$

where L_{in} and L_{out} denote matrices containing pixel locations on the interior and exterior of the level-set, respectively. The switch_in() function (Algorithm 2) moves pixels x from L_{out} to L_{in} if $\widehat{F}(x) > \overline{\widehat{F}}$ and adds neighbouring pixels $N(x)$ to L_{out} via the four connect method (Figure 2.4).

Algorithm 2 The switch_in() function moves pixels x from L_{out} to L_{in} and neighbouring pixels $N(x)$ are added to L_{out} via the four connect method (Figure 2.4).

for x in L_{out} **do**
  if $\widehat{F}(x) > \overline{\widehat{F}}$ **then**
    Add x to L_{in}
    Set $\widehat{\phi}(x) = -1$
    Remove x from L_{out}
    Add $N(x)$ points to L_{in} if $\widehat{\phi}(x) \equiv -3$
  end if
end for

Algorithm 3 The remove_redundant_in() function removes pixels x from L_{in} if the level-set values in the neighbourhood $N(x)$ are all the same

for x in L_{in} **do**
  if N(x) == -1 **then**
    Set $\widehat{\phi}(x) = 3$
    Remove x from L_{in}
  end if
end for

Algorithm 4 The switch_out() function moves pixels x from L_{in} to L_{out} and neighbouring pixels $N(x)$ are added to L_{in} via the four connect method (Figure 2.4).

for x in L_{in} **do**
  if $\widehat{F}(x) < \overline{\widehat{F}}$ **then**
    Add x to L_{out}
    Set $\widehat{\phi}(x) = 1$
    Remove x from L_{in}
    Add $N(x)$ points to L_{out} if $\widehat{\phi}(x) \equiv 3$
  end if
end for

Algorithm 5 The remove_redundant_out() function removes pixels x from L_{out} if the level-set values in the neighbourhood $N(x)$ are all the same

for x in L_{out} **do**
  if all N(x) == 1 **then**
    Set $\widehat{\phi}(x) = -3$
    Remove x from L_{out}
  end if
end for

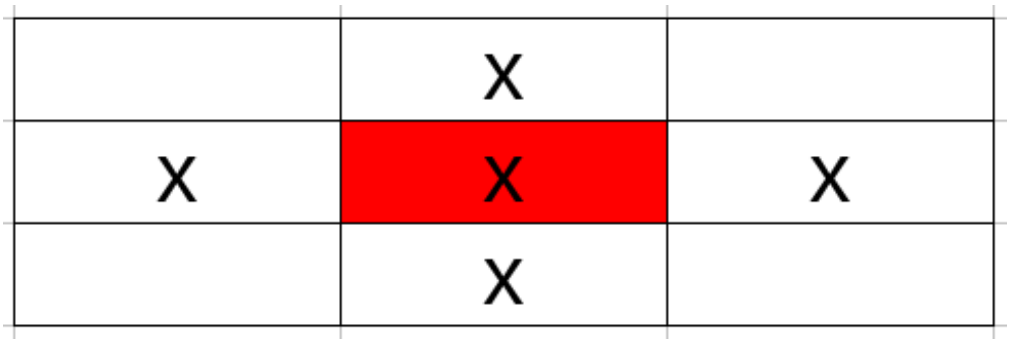

Figure 2.4: 4-connect method for finding neighbouring pixels, where X represents a pixel and the red region is the pixel of interest.

The remove_redundant_in() function (Algorithm 3) removes pixels x from L_{in} if the level-set values in the neighbourhood $N(x)$ are all the same. The switch_out() function (Algorithm 4) removes pixels x from L_{in} to L_{out} if $\widehat{F}(x) < \overline{\widehat{F}}$ and adds neighbouring pixels $N(x)$ to L_{out} via the four connect method. The remove_redundant_out() function (Algorithm 5) removes pixels x from L_{out} if the level-set values in the neighbourhood $N(x)$ are all the same. In summary, I segmented the image with ALSM by expanding and contracting a contour, $\widehat{\phi}$, one pixel at a time around the oocyte. Following successful implementation in oocytes, I transitioned to embryos which are a more complex tissue.

To estimate the volume of the embryo as it underwent osmotic response in real-time, I fitted the contour with an ellipse to smooth the boundary using the fit ellipse function in OpenCV [30]. I estimated the volume of an embryo in three ways: (1) elliptical, (2) spherical, and (3) approximated sphere. For calculating elliptical volume, I used the formula $\frac{4}{3}\pi(\text{minor axis})^2 * (\text{major axis})$. For calculating spherical volume, I approximated the radius of a circle by averaging the major and minor axes of the ellipse, which I used in the formula $\frac{4}{3}\pi(\text{circle radius})^3$. For calculating the approximated sphere, I counted all foreground pixels including the contour boundary as the area of a circle, calculated the radius, and applied it to the spherical volume formula. For manual volume estimates, I used ImageJ to draw and measure an ellipse over the embryo. For each image, a new ellipse was drawn and measured. The volume was estimated using the spherical volume approach.

2.2.5 Statistical Analysis

To test the accuracy of ALSM segmentation I compared it against manual segmentation following Mbogba et al. [124]. I randomly selected 3 images from 10 samples ($n = 30$) using a random number generator in Python. I segmented each image manually and with ALSM to create paired data. To estimate the error in embryo area, I calculated the Dice Coefficient [31, 124]. The Dice Coefficient is a ratio of the intersection between manually and ALSM segmented foreground pixels over the total foreground pixels in both manual and ALSM segmentation [124]. Dice Coefficient values range from 0 to 1, with 0 meaning there is no overlap and 1 meaning there is perfect overlap. To estimate the error in embryo boundary segmentation, I calculated the Hausdorff distance and average absolute distance [124]. The Hausdorff distance estimates

the maximum Euclidean distance between the pixels in the boundary segmented manually and with ALSM [124]. This measures the absolute worst discrepancy between the boundary, a smaller value indicates better agreement between ALSM and manual segmentation [112]. I calculated the average absolute distance for the entire boundary of the embryo [124]. The average absolute distance estimates the average Euclidean distance between the pixels in the boundary segmented manually and with ALSM. This measures average discrepancy between the two boundaries, a smaller value indicates better agreement between ALSM and manual segmentation [112]. I calculated the Dice Coefficient, Hausdorff distance, and average absolute distance in C++ with the OpenCV library [30]. Means and standard deviation are reported for all values unless otherwise specified.

I used the Kruskal-Wallis test to compare between the three methods (elliptical, spherical, and approximated sphere) of estimating volume against manual volume estimation. I then used the post-hoc Dunn test to compare pairwise relationships between all volume estimates and determined which method best approximated manual volume estimation. Results were considered significant if $p < 0.05$. I used the Fisheries Stock Analysis package [135] in R (version 3.6.3, [152]) to perform the Kruskal-Wallis test and post-hoc Dunn test.

2.3 Results

2.3.1 Image Analysis Software

Primate Follicles

I validated the grayscale approximated level-set method (ALSM) prototype on colour images of immature primate follicles provided by Ting and Zilinski (Figure 2.5). Segmentation time ranged from 5 – 10 seconds depending on number, size, and location of the follicles.

Bovine Oocytes

When using the grayscale algorithm for oocytes, the boundary of the oocyte and the image background were too similar for proper segmentation (Figure 2.6a and 2.6b). The colour-based algorithm reduced segmentation time to subsecond rates and improved segmentation accuracy (Figure 2.6c). Smoothing the contour by fitting an ellipse provided the best fit to the true cell boundary (Figure 2.6d).

Bovine Embryos

Embryos had better segmentation capabilities and contrast with the background compared to the oocyte stage (Figure 2.7).

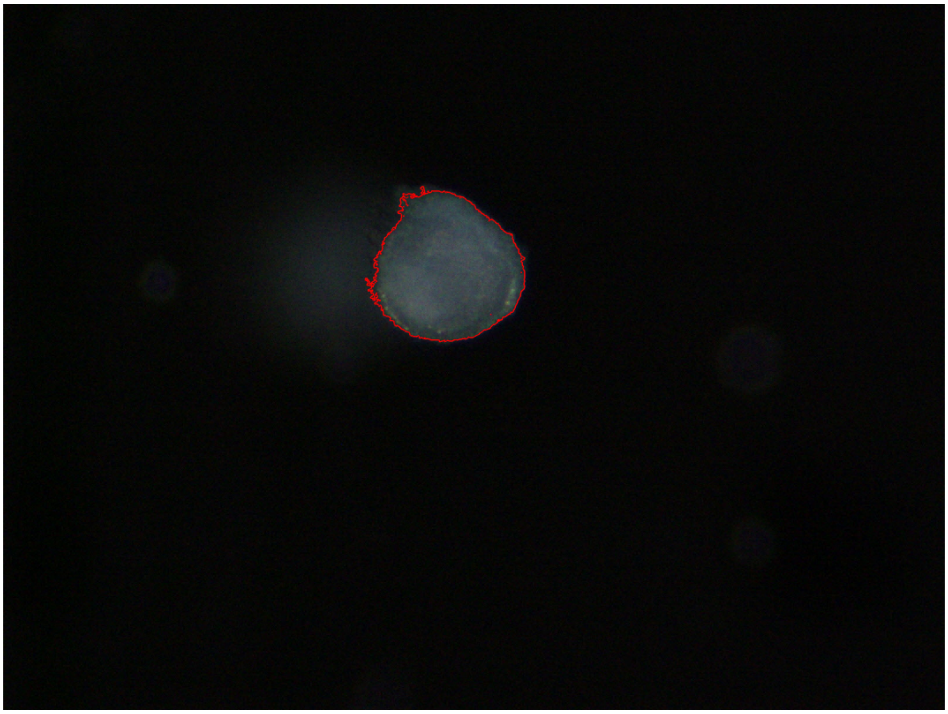

Figure 2.5: Immature primate follicle exposed to 0.5x PBS at 4 °C, segmented (red) with approximated level-set method. Image provided by Ting and Zilinski.

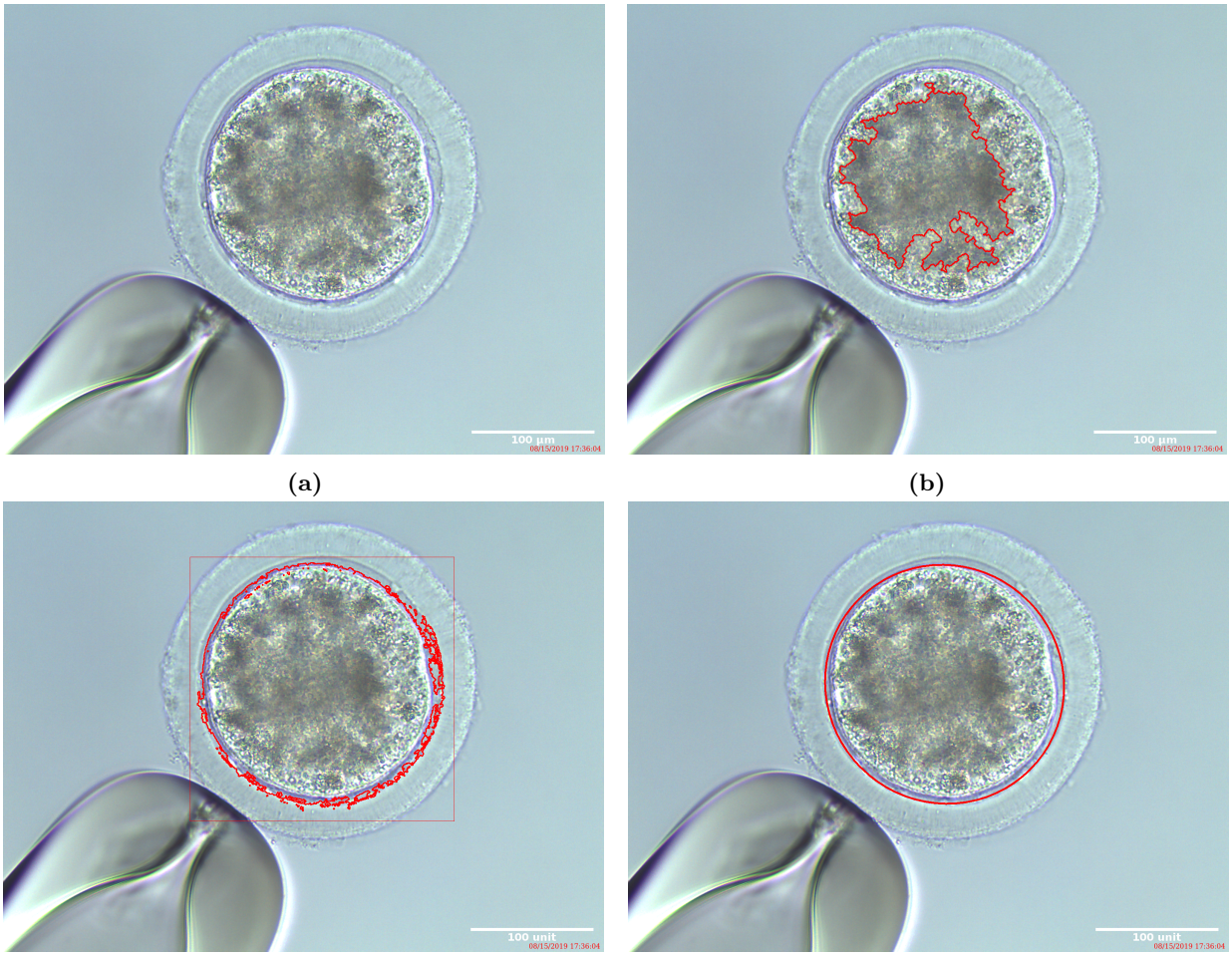

Figure 2.6: Image segmentation developmental stages with colour images of a bovine oocyte exposed to 30% DMSO in 1x PBS. Results of the initial algorithm show in (b). In (c), the mask (red square) was added and speed function was updated from grayscale to colour. The updated speed function shows significantly better segmentation accuracy compared to the grayscale speed function. In (d), an ellipse is fitted to the level-set shown in (c) and the parameters of this ellipse are used to estimate the volume of the oocyte.

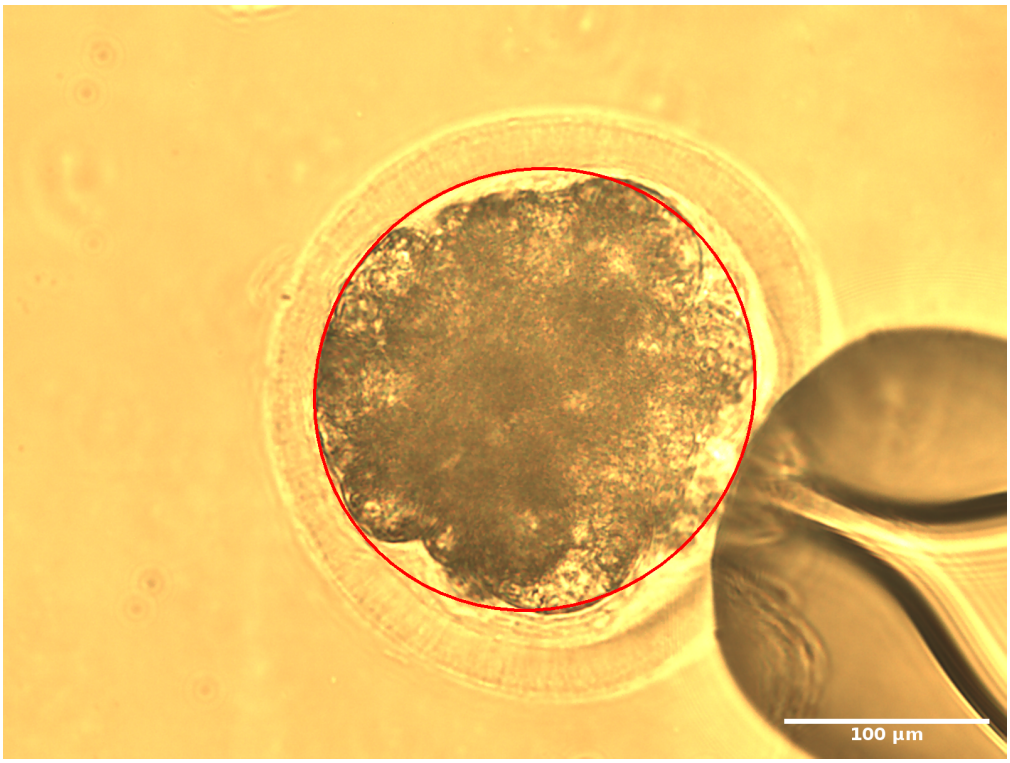

Figure 2.7: Bovine embryo at morula stage exposed to 0.35x PBS and 30% DMSO in 0.35x PBS. Red ring corresponds to segmentation boundary found by fitting an ellipse to the level-set.

The image analysis software segmented images at a rate of 2 frames per second using computer 1 and 0.5 frames per second using computer 2 (Table 2.2). These results corresponded with an average mask (square region around oocyte in Figure 2.6c) of 700x700 pixels. The segmentation time included running ALSM, estimating the volume, displaying analyzed images, and writing data to disk. Manual segmentation on average can be done at a rate of 1 frame every 30 seconds. The ALSM was able to accurately find the area and boundary of the embryos with a mean Dice Coefficient of 0.95 $\pm$ 0.03, mean Hausdorff distance of 19.00 $\pm$ 22.15 pixels, and average absolute distance was 2.98 $\pm$ 8.56 pixels. Through camera calibration, the pixel to μm conversion rate for the Hausdorff distance and average absolute distance yielded 5.80 $\pm$ 6.76 μm and 0.91 $\pm$ 2.61 μm respectively (Table 2.3). The post-hoc Dunn test revealed that elliptical and spherical volumes were the same as manual volume estimates (elliptical: $Z = -0.98$, $p = 0.33$; spherical: $Z = 0.54$, $p = 0.59$, Figure 2.8). Elliptical volume estimates were the same as spherical volume estimates ($Z = -0.44$, $p = 0.66$). There was a difference between the approximated sphere volume and manual volume estimates ($Z = -7.19$, $p < 0.01$).

Table 2.2: Frame rates achieved for each computers used for image analysis.

	Computer 1	Computer 2
OS	Pop OS 20.04 LTS	Raspberry Pi OS
CPU	Intel Core™ i7-8750H	Broadcom BCM 2711
RAM (GB)	16	4
GPU	NVIDIA Quadro P1000 Mobile	NA
FPS	2	0.5

Table 2.3: Comparison results for image segmentation metrics (mean $\pm$ standard deviation).

Embryo	Dice Coefficient	Hausdorff Distance	Average Absolute Distance
1	0.98 $\pm$ 0.01	8.00 $\pm$ 3.61	2.5 $\pm$ 3.05
2	0.93 $\pm$ 0.03	24.43 $\pm$ 8.17	5.58 $\pm$ 9.22
3	0.98 $\pm$ 0.00	3.33 $\pm$ 1.16	0.08 $\pm$ 0.40
4	0.95 $\pm$ 0.06	35.00 $\pm$ 47.63	4.69 $\pm$ 15.38
5	0.96 $\pm$ 0.00	14.08 $\pm$ 8.05	2.96 $\pm$ 6.24
6	0.95 $\pm$ 0.03	6.87 $\pm$ 3.20	0.19 $\pm$ 0.73
7	0.95 $\pm$ 0.01	14.21 $\pm$ 13.12	5.23 $\pm$ 7.77
8	0.90 $\pm$ 0.06	53.77 $\pm$ 36.17	4.70 $\pm$ 14.26
9	0.97 $\pm$ 0.00	10.33 $\pm$ 3.22	0.49 $\pm$ 1.86
10	0.96 $\pm$ 0.01	20.00 $\pm$ 1.00	3.45 $\pm$ 5.88
Average	0.95 $\pm$ 0.03	19.00 $\pm$ 22.15	2.98 $\pm$ 8.56

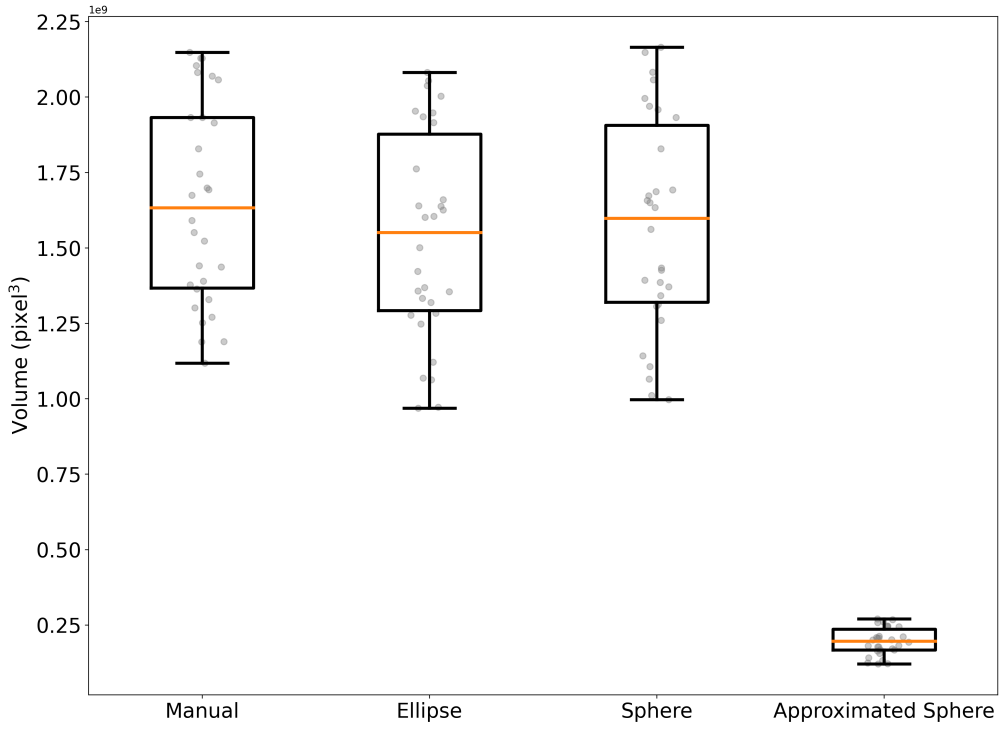

Figure 2.8: Manual, elliptical, spherical, and approximated sphere volume estimates for randomly selected bovine embryos images (N=30). The orange line is the median value, the box represents 50% and the whiskers represent 99.3% of the data.

2.4 Discussion

I sought to create a novel process of real-time image analysis to track the osmotic response of bovine oocytes and embryos during CPA equilibration to reduce osmotic stress. First, I designed a microfluidic device that provided controlled flow of CPA to cells. Second, I modified standard image analysis techniques to analyze colour images in real-time and estimate cell volume. The method I developed advances previous image analysis techniques while creating a novel image analysis system.

My results were focused on using embryos as oocytes are more difficult to cryopreserve. Oocytes are more susceptible to damage during cryopreservation than embryos, some of the contributing factors are: species, developmental stage, origins and significant difference in the cell membrane [147, 182]. Fertilization allows the membrane of an embryo to have better CPA equilibration capabilities and increases osmotic tolerance limits compared to an oocyte, increasing the survivability of cryopreserved embryos [34, 147]. In the future, specific adjustments to address issues specific to oocytes may provide equally promising results to both oocytes and embryos.

The microfluidic device allowed for controlled flow rate directed over the cell. This ensured that new homogeneous media was constantly being delivered to the cell. This follows the design of other microfluidic designs where fresh media constantly passed over the sample area [76, 106, 153, 158]. My microfluidic device

had an open top design which allowed for cells to be suctioned onto a holding pipette and positioned directly in front of the fresh media inlet. The open top design allowed for easy fabrication via 3D printing. Using a holding pipette would theoretically facilitate a more uniform flow of media across the entire surface of the cell as there are no obstructions around the cell, promoting uniform diffusion of CPA across the cell membrane and consequently uniform osmotic response. Other microfludic devices that have been designed to trap cells may have different fluid flow rates around the cell [76, 82, 153]. This may cause non-uniform diffusion of CPA across the cell membrane, which may cause non-uniform osmotic response and aspherical shrinkage. Furthermore, fluid dynamic models can be used to simulate solute concentrations throughout time, allowing for more accurate CPA concentrations to be perfused to the cell [82, 106, 158].

My image analysis software analyzes high resolution colour images in real-time. This was made possible by using a mask (the red square in Figure 2.6c) and a colour based edge function. Other approaches that track objects using the level-set methods have required a difference image [171] or rescaled images [69]. A difference image is when the current frame is subtracted from a reference background image to find an object's boundary. The background image needs to updated over time to maintain an accurate representation of the boundary [171]. Rescaling describes the up- or downscaling of an image's dimensions, which can cause loss of details in the image. My approach avoids both of these issues by finding the tissue boundary directly from the image and masking the image around the tissue. No detail is lost through masking, while maintaining the same speed benefits of rescaling. Image masking also allows for multiple cell or tissue tracking in the future as masking does not affect the original image and each cell or tissue in the image can be masked individually. Unlike with manual segmentation methods my approach saves time and is highly reproducible. Manual segmentation has been known to be both time consuming and error prone [157, 159]. It took me 30 seconds to segment a single image. As I drew a new ellipse for each image, this contributed to the higher per image segmentation time. Time savings are especially important as monitoring CPA equilibration can be done in 15 minutes [76]. For instance, if a cell was being equilibrated with CPA and an image was captured every second, there would be 900 images to analyze over the span of 15 minutes. The manual method would take roughly 10 hours, where as, with my ALSM software it would only take 7.5 minutes.

The approximated level-set method with a colour edge detector showed good segmentation performance. The Hausdorff distance with an average 5.80 μm deviation is small relative to the size of an embryo which has a diameter between 150 to 190 μm including the zona pellucida which had a thickness of 12 to 15 μm [29]. The average absolute distance with an average of 0.91 μm would amount to an average volume estimate error of 0.75 μm^3. Furthermore, the Dice coefficient showed good overlap between manual and ALSM embryo segmentation (Table 2.3) and is in the range of other approaches [124, 194]. Therefore, my method had comparable results to manual segmentation, with fast, accurate, and reproducible results.

By estimating the cell volume during the CPA equilibration, it may be possible to quantify the osmotic stress accumulated by the cell. This is similar to the work Benson et al. [24], who used a toxicity cost function to represent cumulative cell damage due to CPA toxicity. Furthermore, in several trials Dr. Bhat

(post-doctoral fellow) observed that oocytes appeared to stop responding osmotically after 2 or 3 shrink swell cycles. This new observation suggests that a number of new hypotheses can be explored with this new approach.

Real-time image analysis is the first step to obtaining a volumetric optimized cryopreservation approach. In order to exchange water and CPA at a 1:1 ratio as proposed by Levin and Miller [102], extracellular CPA concentrations must be coupled with cell volume. The adjustment to extracellular CPA concentration can be done using feedback control, specifically a Proportional-Integral-Derivative (PID) controller. Outside of cryobiology, PID controllers have been successfully used to perfuse drugs in live animals [113]. Mage et al. [113] demonstrated that PID controller could compensate for individual variation, was able to maintain target concentrations over 95% of the time, and can be applied to a wide range of animals. This implies that a volumetric approach using a PID controller could equilibrate cells or tissues with CPA without any prior experimentation and that individual variations in membrane biophysics would be automatically compensated for. This is possible as the PID controller computes error, the difference between the cell or tissue's current volume (using ALSM) and isotonic volume (also using ALSM), which is then used to determine, increase or decrease, extracellular CPA concentration in order to maintain an isochoric state.

Therefore, the next step for obtaining a volumetric optimized approach is to implement a PID controller, while coupling it with my microfluidic device and image analysis software. A volumetric optimization approach has potential as an empirical process, and the goal of reducing osmotic stress and cytotoxicity for oocyte and embryo cryopreservation may be achieved.

3 Optimization of Media for Sperm Cryopreservation

3.1 Introduction

3.1.1 Media Optimization

While volumetric optimization (Chapter 2) is a reasonable approach for improving the cryopreservation process for increased functionality and viability of oocytes and embryos as they are non-motile and easily observed for image capture and analysis, sperm require a different approach due to their motility. Instead, I will focus on optimizing the composition of cryopreservation media (CPM) to increase the functionality of post-thaw sperm. Sperm cryopreservation was first successfully performed when glycerol was used as a permeating cryoprotectant (CPA) [144]. Following this success, optimization of the sperm cryopreservation process was done empirically, leading to the use of egg yolk to protect sperm from thermal damage and increasing post-thaw survival [137, 192].

Sperm cryopreservation still has many challenges. In general, $40 - 50\%$ of sperm do not survive the cryopreservation process even with optimized protocols [16, 24, 189]. There is inter and intra bull sperm variation that lead to variation in post-thaw parameters, such as post-thaw motility [16]. Seasonal variations have an effect sperm quality [114]. Individual genetics contribute to the heterogeneity of sperm as they impact sperm morphology [16, 117]. These are only some of the many factors that have an effect sperm parameters. Recent empirical studies showed that pre-freeze motility of greater than 70% corresponded with post-thaw motility rates between 50 to 68%, depending on the cryopreservation media used, species, sample, donor, and many other factors [16, 27, 92].

Conventional cryopreservation of cultured cells can be done using very few ingredients such as a buffer which maintains the pH and salinity for the cell, and a permeating CPA such as dimethyl sulfoxide (DMSO) [2, 146]. Permeating and non-permeating CPA provide physical and chemical protection to sperm during the cooling, freezing, and thawing process [16, 180]. However, sperm cryopreservation requires multiple media components as the mechanical functionality of sperm must be preserved (Table 3.1) [10, 24, 33, 180].

Along with the extensive list of components needed for proper freezing of sperm, there are complex interactions between media components and freezing protocol [33, 44, 196]. For example, certain CPAs become less toxic as temperatures decrease, thus introducing a high concentration of CPA may be done at subzero temperatures to avoid toxicity [25, 192]. Pollock et al. [146] determined that optimal CPA concentration interacts with optimal cooling rates. Depending on the cell being cryopreserved, they found

Table 3.1: The media components used by Chaveiro et al. [33] to explore the influence of salt-based and sugar-based (tris versus sucrose) freezing media on sperm post-thaw viability. Table redrawn from [33] to contain only a single media composition.

Media components	Mode of action
Tris	Base media
Citric acid	Base media
Sucrose	Non-permeating cryoprotectant
Fructose	Energy source
$NaHCO_3$	Ph balance
Glycerol	Permeating cryoprotectant
Equex	Detergent
Sodium penicillin	Antibiotic
Streptomycin sulfate	Antibiotic
Egg yolk	Membrane stabilizer

the optimal CPM composition and corresponding cooling rate for various cultured cell types (Jurkat and mesenchymal stem cells) [146]. Thus, component interactions need to be considered when finding the optimal CPM composition.

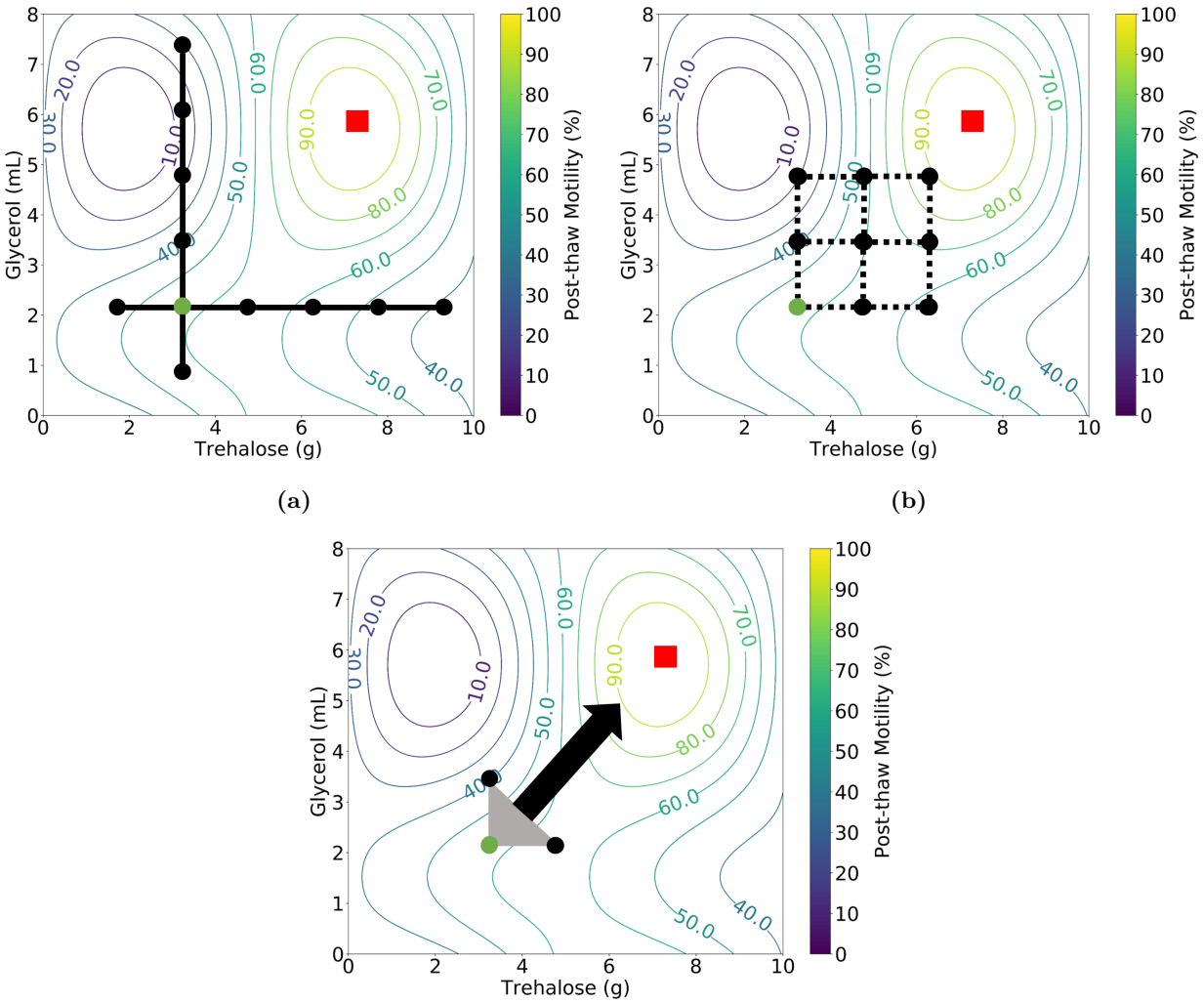

Figure 3.1: Optimization strategies applied to a hypothetical model dependent on trehalose and glycerol: (a) One-variable at a time, (b) factorial, and (c) gradient. The green dot represents a starting location, the black dots are sampling points, and the red square is the optimal. The one-variable at a time method is an iterative optimization approach that finds the optima in one variable while holding all others constant. The factorial method samples points in a grid and selects the best result as the optimal. The gradient approach uses the sample point results to suggest the direction of the optimal.

To explore these interactions and find the optimal composition of CPM, there are three classical approaches that have been used: (1) one-variable at a time, (2) factorial, and (3) gradient (Figure 3.1). The one-variable at a time strategy finds the optimal value for each variable in the experimental design iteratively [13, 61]. For example, Chaveiro et al. [33] improved the freezing protocol for bovine sperm by optimizing the components of the freezing media, then explored the effects of cooling rate at different steps in the protocol. However, this experimental design can be very resource intensive as the number of experiments increase exponentially with the number of factors [13, 61]. Furthermore, variable interactions are not considered with this experimental design [61].

The factorial strategy involves testing all combinations of design variables then selecting the best resulting combination as the optimal. For instance, Dong et al. [44] used a four-way factorial design to explore interactions between pre-cooling rates (bring sample temperature to 4 °C for CPA equilibration), CPA, cooling (decrease temperature from 4 °C to −80 °C), and thawing rates for sperm cryopreservation in rhesus monkeys (*Macaca mulatta*). They used a four-way factorial design: CPA (4 levels), pre-cooling rates (2 levels), cooling rates (4 levels), and thawing rates (2 levels). This led to 64 conditions ($4 \times 2 \times 4 \times 2$) that were tested in triplicates. Then, to test all conditions 1-3 sperm samples per monkey were divided into 192 freezing straws, for a total of 192 straws per monkey. Given the large number of samples required for a full factorial design, this approach is both time and resource intensive. The factorial strategy is also limited in the number of levels that can be tested for each factor, which restricts the experiment to a smaller field of possible trials.

Gradient strategies aim to find the optimum by observing the rate of change in the response variable as the experimental variables change [134]. The optimum is assumed to be reached when this rate of change stops. In this case, post-thaw motility of sperm is the response variable, while the components of CPM are the experimental variables. For the gradient strategy, local response variable data is required a priori. The rate of change can be approximated or a continuous, differentiable, and smooth model can be fitted from a priori data (e.g. a quadratic model) [42, 110]. For example, a quadratic polynomial model is a continuous, differentiable, and smooth model as it does not have any abrupt changes in the response value and the rate of change can be estimated everywhere. Then, the maximum or minimum can be found by determining when the rate of change in the response variable is zero [42]. Determining optima and validating using the gradient strategy is most easily achieved when the theoretical model is continuous and differentiable, for example, a response surface.

Response surface methodology is a popular method for optimizing multivariate problems [42, 110], and has recently found its way into cryobiology [73, 153]. Response surface methodology uses statistical and mathematical techniques to fit the response variable of interest, y, to the experimental design parameters, $x_1, \ldots, x_n$ as follows,

$$y = f(x_1, \ldots, x_n) + \epsilon, \tag{3.1}$$

where f is the response function to approximate and ϵ represents random variability not included in the

response function [131]. Han et al. [73] used response surface methodology to increase viability of freeze-dried bacteria by finding the optimal CPM composition. However, this method proved to be as time and resource intensive as the factorial optimization strategy.

Therefore, as classical optimization strategies (one-variable at a time, factorial, and gradient) are limited for the optimization of freezing media, here I used a modified version of the gradient strategy to construct a differentiable function. Then, I used novel machine learning techniques coupled with an optimization algorithm to guide the selection of optimal cryopreservation media to increase post-thaw motility in bovine sperm.

3.1.2 Machine Learning

Machine learning is a set of algorithms that allows for a computer to learn a set of rules or a model from a dataset [7, 67]. Machine learning improves its operation over time as the algorithm gains experience and tunes the predictions to improve model performance. Machine learning has been used directly in media optimization [13, 42]. For example, Ba and Boyacyi [13] and Desai et al. [42] used artificial neural networks, a type of machine learning model, to compare against traditional models used in chemical reaction kinetics and media optimization respectively. Artificial neural networks (ANN) are a"black-box" model, where the input and output are observable and the inner works are unknown (Figure 3.2) [131]. For example, Desai et al. [42] ANN had four inputs: sucrose, yeast extract, K_2HPO_4, and $MgSO_4$ and one output, yield. Artificial neural networks are able to approximate explicit models (e.g. second-order polynomial) without specifying the model a priori [13, 83]. This means that assumptions such as: the model should be linear, the variable interactions should be quadratic, or the model should be exponential do not need to be specified before creating and training the ANN [7, 13, 42].

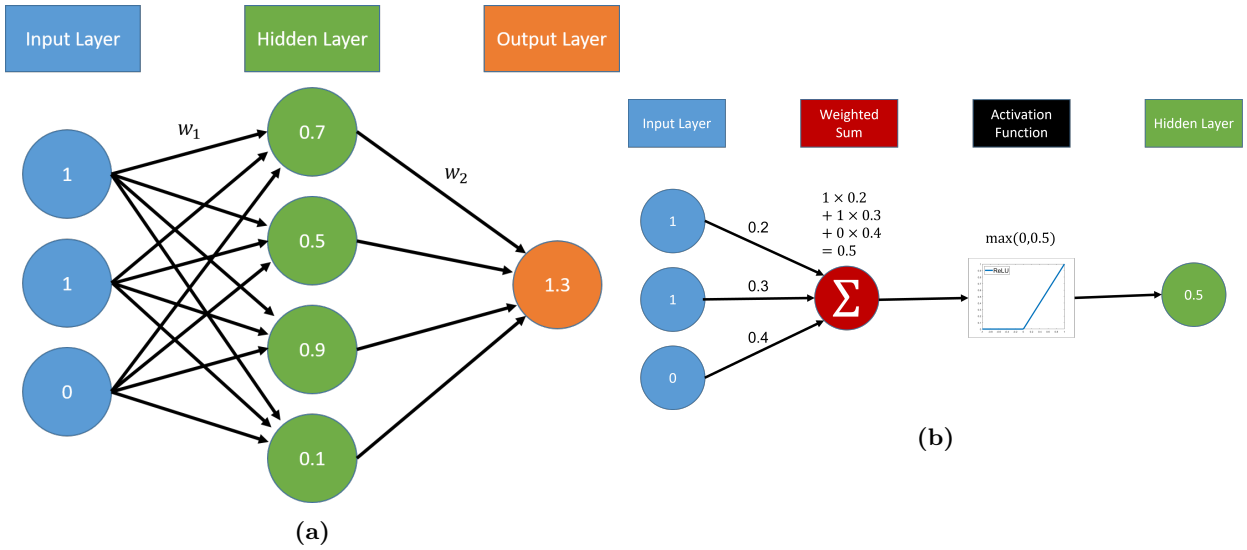

Figure 3.2: Format of an artificial neural network (a) with 3 input nodes, referred to as neurons, 4 neurons in the hidden layer and 1 output neuron. The weight parameters w_1 and w_2 are real numbers and are optimized during training. Values in the hidden layer are calculated (b) via a weighted sum, then passed to an activation function that determines the value of the node in the hidden layer. Figure redrawn from Angermueller et al. [7].

A second type of machine learning, Gaussian process regression (GPR), has been used in optimization tasks [126]. The Gaussian process regression is built on a Gaussian process, which is a collection of random variables such that the collection has a joint Gaussian distribution [155]. Morschett et al. [126] used GPR to analyze and visualize the nonlinear relationship between media composition and lipid productivity. With the GPR model Morschett et al. designed further experiments to locate the optimal media composition [126]. After training the GPR they required 4 more rounds of testing to determine the optimal media composition [126].

As machine learning is a relatively new technique, the application of multiple methods should be explored. Although ANN and GPR have been used in media composition optimization, it has yet to be determined how these two machine learning options may perform in contrast when optimizing media composition.

3.1.3 Differential Evolution

Differential evolution (DE) is an iterative data-driven optimization algorithm that is based on biological evolution mechanisms [149]. Differential evolution directly compares a starting population to a mutated population and selects the best individuals within both populations based on fitness for the next iteration [149]. The process is iterated until the fitness of the population converges, for instance, the same best member in a population is observed over multiple generations or when the generational average plateaus [142, 146, 149]. Iterative data-driven optimization methods have been used to optimize media composition [146]. Pollock et al. [146] were the first to apply DE to optimize media composition and cooling rate of cultured Jurkat (white blood) cells and mesenchymal stem cells. The results showed that two cell types had

different optimal cryopreservation protocols and media compositions [146]. As Pollock et al. [146] used DE to optimize cryopreservation media compositions and protocols in two different cell types, it suggests that DE is a suitable strategy for sperm cryopreservation optimization given that sperm response to cryopreservation is known to vary both between and within bulls [80, 117].

3.1.4 Objectives

The purpose of this study was to use a novel, data-driven optimization technique to optimize post-thaw motility in bovine sperm. I had two central objectives:

1. As machine learning is a relatively new technique to optimize cryopreservation protocols, to determine which of two methods (artificial neural networks and Gaussian process regression) offered more precise estimation of theoretical post-thaw motility

2. Once the preferred machine learning method had been determined, to couple theoretical and empirical testing to optimize cryopreservation media composition for improved post-thaw motility in bovine sperm.

3.2 Methods

The process to optimize CPM composition for improved sperm motility following cryopreservation is a complicated approach that involves theoretical modeling and empirical testing. Although each section is written separately, it should be understood that each section is integrated into the overall process and occurs concurrently. A figure has been included to illustrate the process (Figure 3.3).

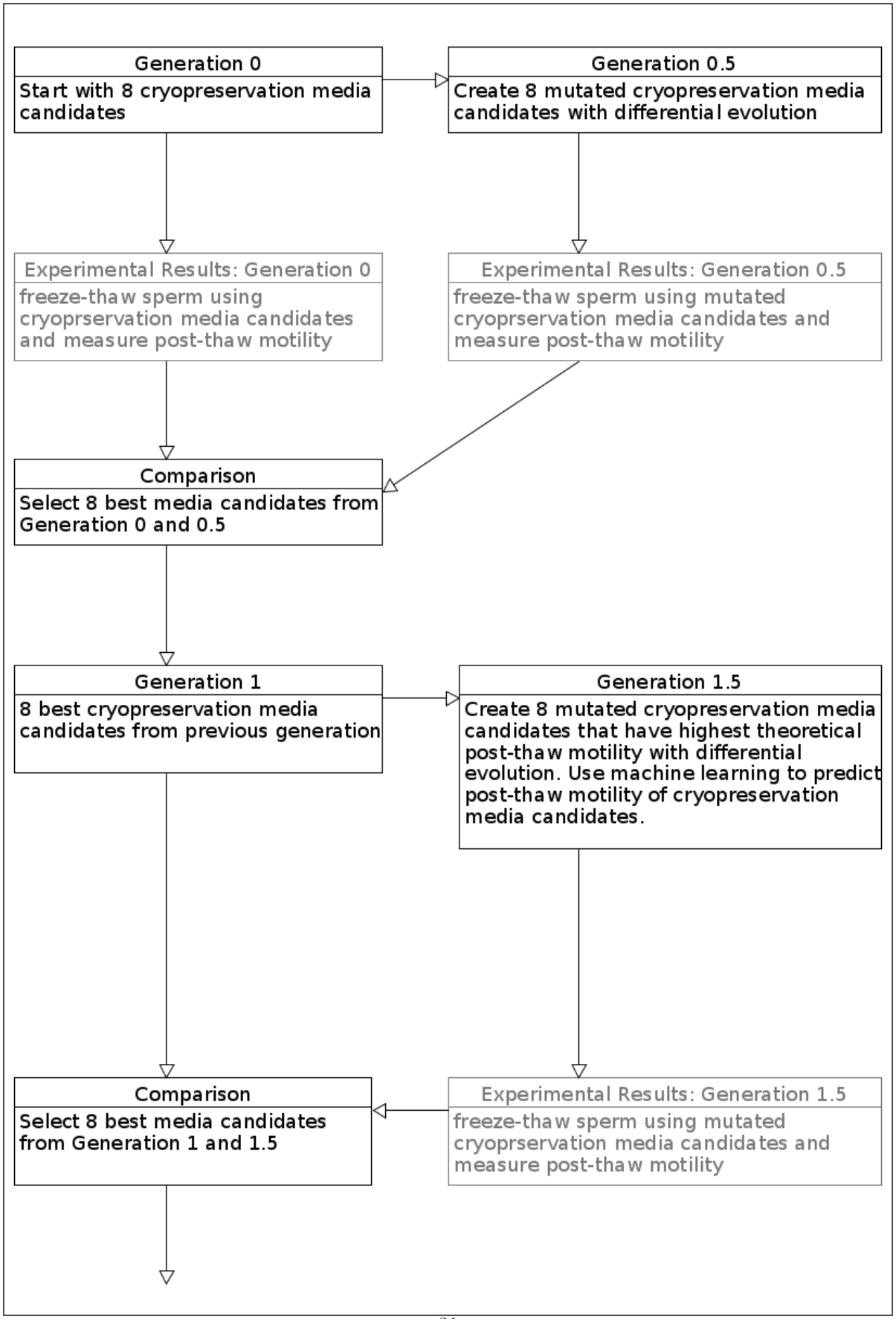

Figure 3.3: Schematic of optimization approach.

3.2.1 Empirical Testing

For each empirical test of CPM composition, semen was collected from 4 bulls that were randomly chosen from a larger herd (>100 bulls). Semen was collected by artificial vagina from Holstein bulls at Semex (Quebec, Canada). Before any processing, the sperm quality was assessed for volume, colour, and contamination of urine and blood. The semen was held in a water bath at 34 °C while the sperm concentration, initial percentage of motile sperm, and percentage of non-normal morphology were estimated. Sperm concentration was estimated by optical density using a calibrated spectrophotometer. The percentage of motile sperm and non-normal morphology was estimated at 34 °C by subjectively examining several fields of diluted semen projected on a television monitor connected to a microscope. Concentrations of at least 1×10^9 sperm/mL, motility of at least 70% and maximum non-normal morphology of 10% were considered acceptable for experimentation. Each sample from each bull was divided into 4, as 4 experimental CPM compositions were tested concurrently. There were no replicates of sampling within bulls for each CPM composition.

For each experimental CPM composition, the semen was diluted to a concentration of 1×10^8 sperm/mL using CPM, where the proposed media components investigated are listed in Table 3.2. Following the addition of CPM, semen was loaded into 0.25 mL straws. The straws were sealed, and the semen was frozen within 24 hours. The straws were cooled at approximately −15 °C/min from 6 °C to −100 °C. Then the straws were transferred to a liquid nitrogen tank and stored until thawed.

Table 3.2: List of components used in the cryopreservation media and initial concentration ranges. All cryopreservation media contained water, a component dependant on the concentrations of other components.

Component	Mode of Action	Initial Concentrations	Citation
Tris	Base media	$0 - 50\%$	[118]
Egg yolk	Membrane stabilizer	$0 - 20\%$	[118, 137]
Milk	Membrane stabilizer	$0 - 15\%$	[5]
Fructose	Energy source	$0 - 1.25\%$	[5]
Glycerol	Permeating cryoprotectant	$0 - 7\%$	[12]
Ethelene Glycol	Permeating cryoprotectant	$7 - 9\%$	[170]
Trehalose	Non-permeating cryoprotectant	$0 - 100$ mM	[35, 38]
Cholesterol Loaded Cyclodextrin	Membrane stabilizer	$0.5 - 1 \frac{\text{mg}}{\text{ml}}$	[151]
Glutathoine	Enzymatic antioxidant property	0.5 mM	[81, 163, 197]
Melatonin	Antioxidant	$2 - 3$ mM	[10]
Nerve Growth Factor	Growth factor	$0 - 0.5 \frac{\text{mg}}{\text{ml}}$	[160]

Once thawed, computer-assisted sperm analysis (CASA), which uses image analysis, measured post-thaw motility in the sperm samples [175]. The estimations provided by CASA are considered as reliable as manual

methods [175]. This process was repeated on 4 bulls to test 4 additional experimental CPM compositions. The 8 compositions together were considered 1 generation of the optimization model (Figure 3.3). Each sample was also processed with commercial media to serve as a control against the empirical tests.

3.2.2 Theoretical Testing

To answer my first objective, I used two machine learning methods that can be trained using supervised learning: artificial neural networks (ANN) and Gaussian process regression (GPR). I created both ANN and GPR models in Python using TensorFlow and Scikit-Learn modules respectively. I used K-fold cross validation to train and test the machine learning models. I partitioned the dataset that contained data from all 9 generations ($n = 327$) 10 fold, with 9 partitions used as training data and the remaining partition used as testing data (Figure 3.4) [48].

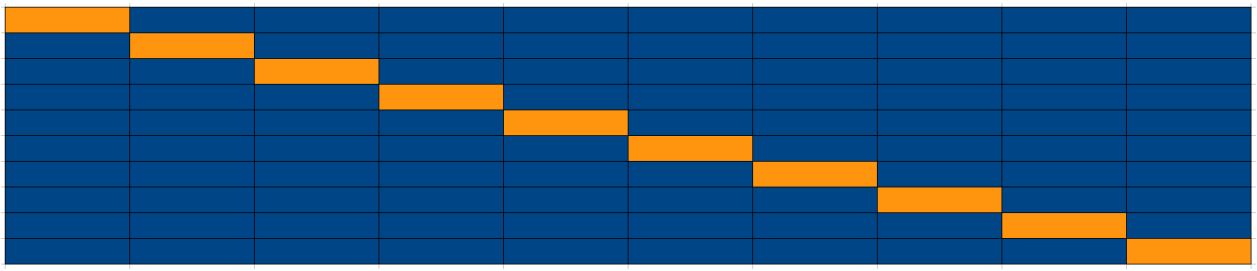

Figure 3.4: 10-fold cross validation partitioning a dataset into training (blue) and testing (orange) datasets.

I trained the ANN using a back-propagation routine [7, 198]. I introduced the experimental data to the ANN, where it predicted the output. I then compared the predicted output to the experimental output with an error function that produced an error estimate. The error estimate was propagated backwards through the ANN and modified the connections between the nodes to improve the model. I considered the ANN trained when the mean squared error (MSE) for a given function was minimized. The optimal ANN was obtained by modifying the number of hidden layers and the number of neurons in each hidden layer (Figure 3.2a). I used a factorial search with the number of hidden layers and number of nodes per hidden layer as factors to find the optimal ANN, the one with the lowest MSE [53, 83]. I used the formula by Feng and Yang [53] to determine the number of nodes per layer. The number of hidden layers ranged between 1 to 3 and the number of neurons per hidden layer ranged between 4 to 18. As the number of hidden layers and neurons increase, so does model complexity [7]. An ANN that is too complex could result in overfitting [7]. Overfitting occurs when an ANN has high prediction accuracy with training data and low prediction accuracy with testing data. That is, an overfit model would produce inaccurate post-thaw motility predictions and I accounted for overfitting through regularization. Just as for ANN, I trained the GPR model using the experimental data and predicted post-thaw motility. The GPR was fitted using all default values provided by Scikit-Learn. The GPR model was trained using maximum likelihood estimation.

Both models will predict the post-thaw motility for CPM compositions in the testing subset. Then the experimental post-thaw motility from the same dataset along with the corresponding predictions were used to calculate MSE. The lower the MSE, the better the prediction. I used the average MSE from the testing dataset generated by 10-fold cross validation to compare ANN to GPR. As new experimental data became available, I used it to continuously improve the predictions of post-thaw motility.

3.2.3 Differential Evolution

To optimize the composition of CPM that were tested theoretically and empirically, I used differential evolution (DE). The algorithm for DE starts with x a real valued matrix, with elements of the form $x(\text{CPM Component}, \text{CPM Number})$. Generation 0, consisted of eight CPM compositions that were generated using the initial concentrations listed in Table 3.2. Beginning with generation 0, denoted as x_0, I mutated x_0 to create $\widehat{x}_0$ by the following rule,

$$\widehat{x}(i,j) = \begin{cases} x(a,j) + K\left(x(b,j) - x(c,j)\right), & \text{if } \eta > CR \\ x(i,j), & \text{otherwise} \end{cases} \tag{3.2}$$

where $\eta \sim N(0,1)$ is a random number drawn from the Normal distribution with mean 0 and variance 1, a, b, c are random integers in the interval $[1, \text{Number of components in CPM}]$, $K \in [0,1]$ is a scaling factor. The crossover rate, CR allows for previous results to propagate to the next generation. In order to begin the DE algorithm, eight initial CPM composition were provided to Semex to serve as generation 0. I then propagated eight mutated compositions, generation 0.5 (Figure 3.3). Both sets of eight were tested empirically at Semex. I compared the sixteen motility results from the CASA report and chose the eight compositions that performed best in the experiment (generation 1).

From here I used an iterative approach from generation 1 to generation n to achieve an optimized CPM composition using a combination of empirical and theoretical tests (Figure 3.3). I used DE to create an additional eight compositions. I then used machine learning (Section 3.2.2) to determine the theoretical fitness (motility) of these eight compositions. I used these theoretical fitness results to guide DE by selecting mutated CPM compositions that were predicted to have a higher post-thaw motility then the original CPM compositions. I repeated the process of determining theoretical motility to guide additional sets of CPM composition until a large dataset was created. From this, I determined the eight best compositions (generation 1.5) of CPM for sperm motility. These eight theoretical CPM compositions were tested empirically at Semex. I compared the motility of the empirical results from the CASA report to the theoretical generation 1 and selected the eight CPM compositions that performed best to become generation 2. I then repeated this process for 9 generations until the post-thaw motility from one generation to the next was within a tolerance of 10^{-1}, referred to as convergence. Until enough data was gathered to produce an acceptable machine learning model, a uniform random number generator was coupled to the DE algorithm to predict optimal CPM compositions. Specifically, the uniform random number generator was used to predicted the fitness of

each CPM compositions produced by DE, only mutated CPM compositions with higher fitness were kept. When the machine learning model matched the experimental data at an acceptable level, I coupled the model at generation 6 with the DE algorithm to predict optimal CPM compositions.

3.2.4 Statistical Analysis

I completed all statistical analysis in R (version 3.6.3, [152]) using the FSA: Fisheries Stock Analysis package [135]. To test the predictive ability of the machine learning models, I used Kruskal-Wallis test to compare experimental results, commercial results, ANN predictions, and GPR predictions. I used generation 9 for the comparison ($n = 32$). I then used a post-hoc Dunn test to test pairwise relationships between all four datasets and determine whether ANN or GPR best approximated the response surface generated by the experimental results. To test for convergence of the DE algorithm I used Kruskal-Wallis test to compare the experimental results from generations 7, 8, and 9 ($n = 96$). Comparisons were considered significant for $p < 0.05$. Means and standard deviation were reported for all values unless otherwise specified.

3.3 Results

3.3.1 Optimal Theoretical Model

I used 328 cryopreservation media post-thaw motility pairs to train and test the machine learning algorithms. All artificial neural networks (ANN) had 12 input neurons and 1 output neuron. The first ANN had 12 neurons (one for each input), one hidden layer, and had an average MSE of 390. The ANN with the lowest average MSE had 10 neurons per hidden layer, 2 hidden layers, and an average MSE of 373 (Figure 3.5). The Gaussian process regression (GPR) had an average MSE of 745 on the testing dataset. The ANN has less prediction error then the GPR.

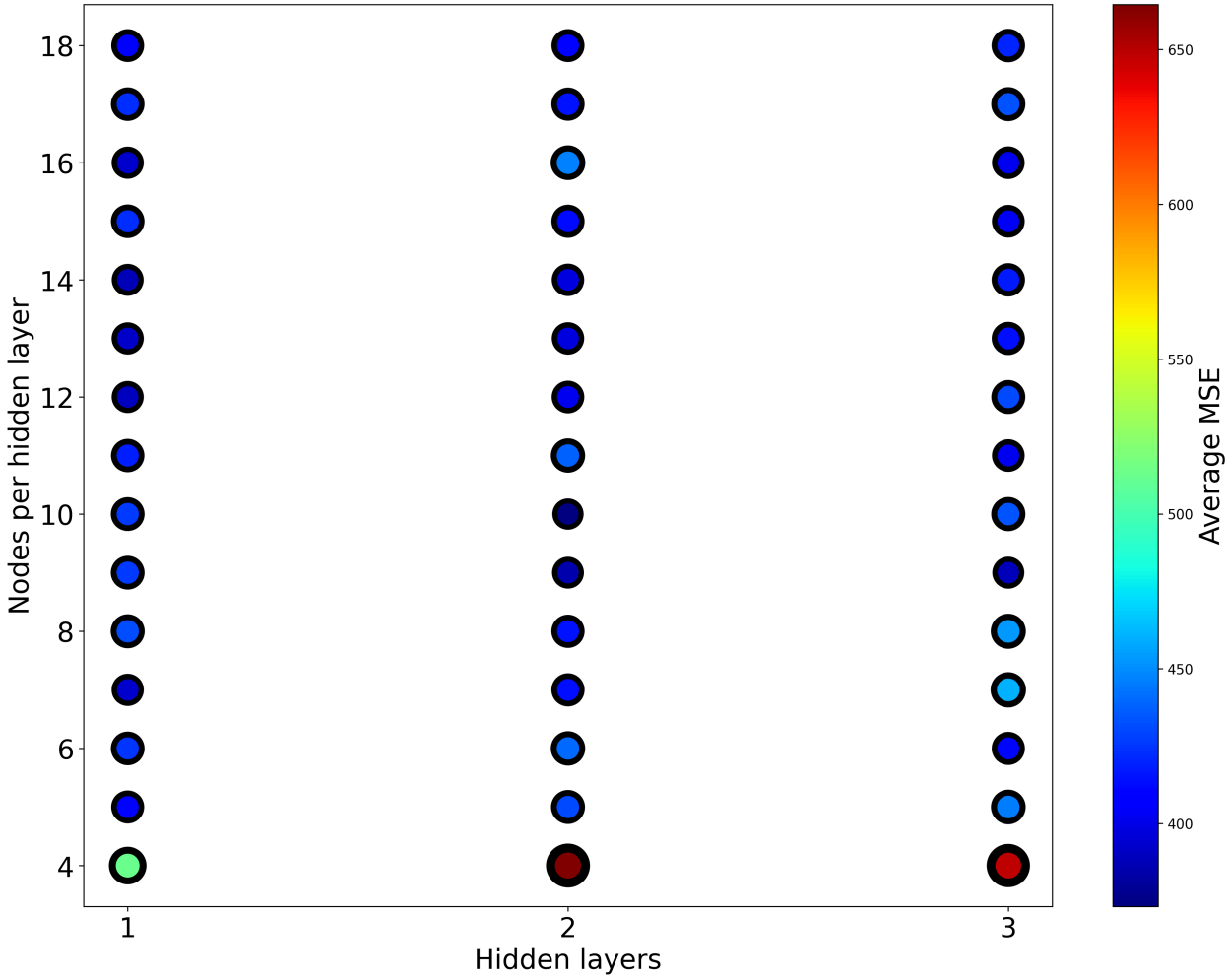

Figure 3.5: Exploring the relationship between the number of hidden layers and the number of nodes per hidden layer. From 10-fold cross validation, the artificial neural network with the lowest average MSE of 373 had 2 hidden layers and 10 neurons per hidden layer.

The median values for the ANN predictions, GPR predictions, experimental, and commercial results were $(41.93 \pm 3.52)\%$, $(54.85 \pm 6.26)\%$, $(54.47 \pm 17.37)\%$, and $(67.10 \pm 13.38\%)$ respectively. There was a statistical difference detected between ANN predictions, GPR predictions, experimental results, and commercial results ($\chi^2 = 36.20$, $df = 3$, $p < 0.01$). The post-hoc Dunn test revealed GPR predictions and experimental results were not different ($Z = -0.03$,$p = 0.96$). No difference was found between GPR predictions and commercial results ($Z = 1.37$,$p = 0.17$). However, there was a difference between the ANN predictions and experimental results ($Z = -4.32$,$p < 0.01$), as well as, commercial results ($Z = -5.57$,$p < 0.01$). A difference was found between ANN predictions and GPR predictions ($Z = -4.34$,$p < 0.01$). Thus, GPR better approximated the post-thaw motility response surface compared to ANN (Figure 3.6).

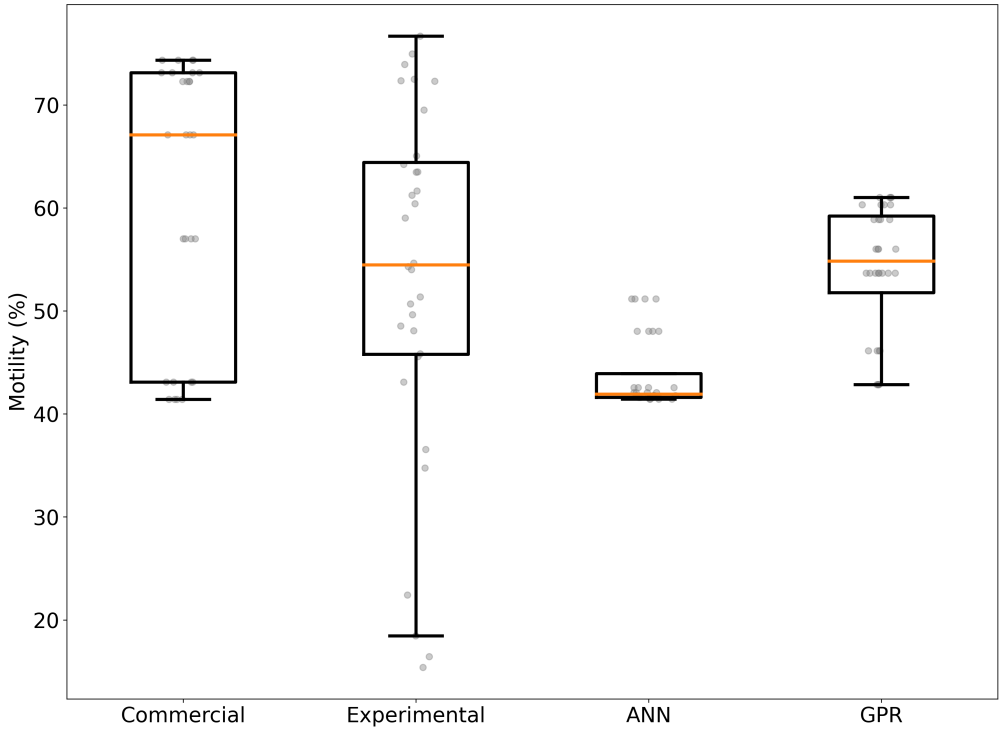

Figure 3.6: Post-thaw motility predictions from artificial neural network and Gaussian process regression and experimental and commercial results from generation 9. The MSE the artificial neural network was 373 and 745 for the Gaussian process regression. Dots are individual bull post-thaw motility values. The orange line is the median value, the box represents 50% and the whiskers represent 99.3% of the data.

3.3.2 Optimal Media Composition

The mean post-thaw motility from generation 1 to 6 increased from $(26.54 \pm 20.3)\%$ to $(43.40 \pm 16.49)\%$ based solely on differential evolution. After coupling differential evolution with GPR the mean post-thaw motility increased from $(51.42 \pm 6.97)\%$ at generation 7 to $(53.14 \pm 17.37)\%$ at generation 9. The coupled algorithm was able to reduce the number of CPM compositions that produced suboptimal post-thaw motility (Figure 3.7).

The median post-thaw motility for generations 7, 8, and 9 were 52.57%, 55.99%, and 54.47% respectively. The convergence testing between generations 7, 8, and 9 indicated that there were no differences between the three generations and the algorithm is approaching a set optimal CPM compositions ($\chi^2 = 1.73$, $df = 2$, $p = 0.42$). Furthermore, sperm cryopreserved in experimental media had the same post-thaw motility as sperm cryopreserved in commercial media ($Z = 1.40$,$p = 0.16$, Figure 3.6). A comparison of media from generation 9 to commercial medium (Figure 3.8) showed media trials 65 to 68 had mean post-thaw motility that was (31 ± 21)% below commercial and media trials 69 to 72 had mean post-thaw motility that was (13 ± 22)% above commercial.

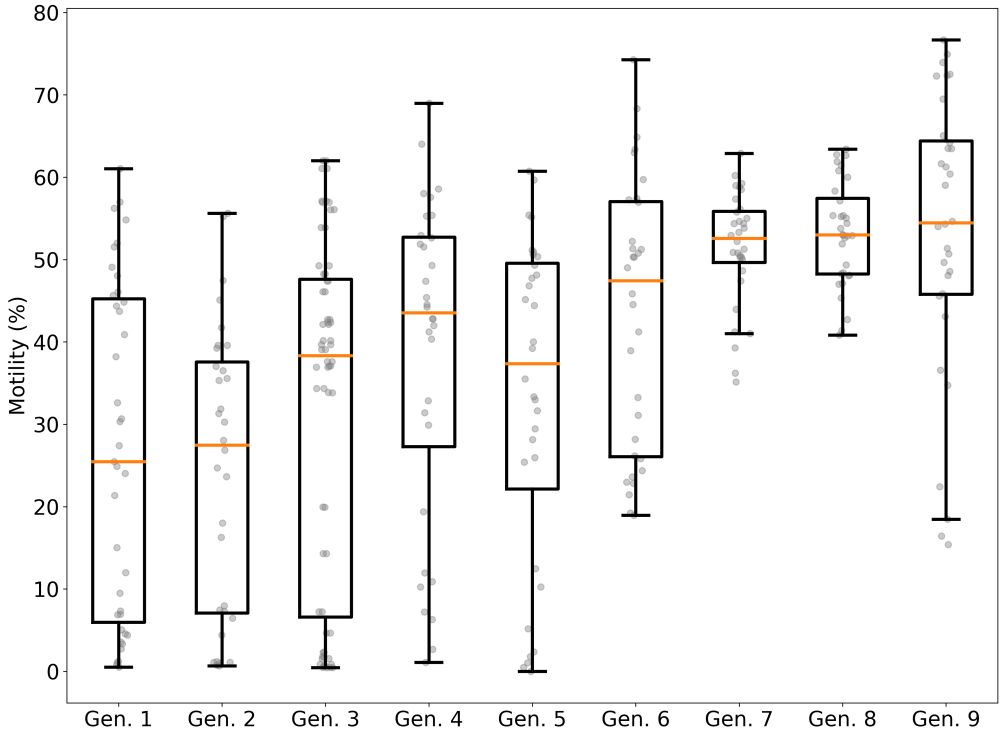

Figure 3.7: The post-thaw motility of sperm cryopreserved with media generated by differential evolution before coupling with Gaussian process regression at generation 6 and after coupling Gaussian process regression at generation 7. The orange line is the median value, the box represents 50% and the whiskers represent 99.3% of the data.

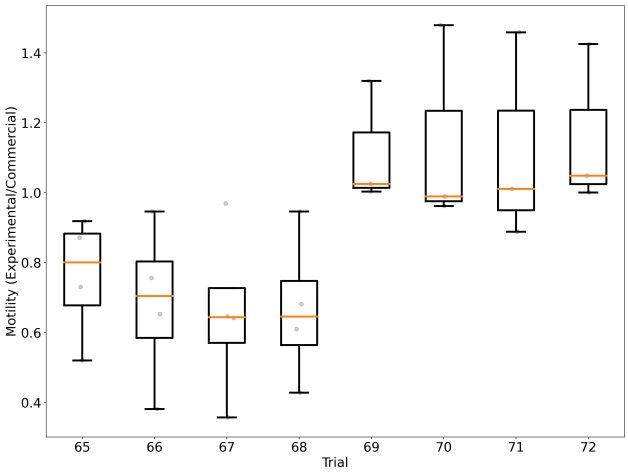

Figure 3.8: Direct comparison of media generated by differential evolution to commercial medium for media from generation 9 to commercial media. The ratio of experimental post-thaw motility over commercial post-thaw motility represents post-thaw motility gain or loss depending on the media composition. The orange line is the median value, the box represents 50% and the whiskers represent 99.3% of the data.

3.4 Discussion

I sought to optimize post-thaw motility in bovine sperm through a novel data-driven approach. First, I determined that GPR performed better then ANN for predicting empirical results. Second, the cryopreservation media composition optimized through data-driven algorithms performed at a level comparable to traditional commercial media. The method I developed advances previous techniques, while also creating an entirely novel system for cryopreservation optimization.

3.4.1 Optimal Theoretical Model

My first objective was to determine which machine learning model (artificial neural networks and Gaussian process regression) offered more precise estimation of theoretical post-thaw motility. Overall, the ANN had reduced error compared to the GPR and therefore had more precise theoretical estimates of post-that motility. Upon comparison to the empirical results the post-thaw motility, the GPR out-performed the ANN.

The reason that ANN may have underperformed compared to GPR is due to increased variability. For example, two studies have shown that artificial neural networks appear to be most successful when the variability in the data was smaller [13, 42]. In both of these studies the variability of the data was smaller. The variability in my data comes from the random sampling of bulls for each CPM trial to account for the inter and intra bull sample variation [16, 36, 60, 117], as genetic differences cause large variations in sperm morphology between and within individuals [117, 173]. Seasonal fluctuations also influence sperm freezing capabilities [114]. Therefore, individual genetics and season variation are some factors that cause post-thaw motility to be less precise [16, 80, 114]. There is a trade off between precision and accuracy that is made

when finding the optimal theoretical model.

The amount of variation within the biological system being modeled should be a factor in finding the optimal model. With ANN being more precise, biological systems with high inter and intra sample variation may indicate using models that are more accurate and factor variation into their predictions. For instance, cultured Jurkat cells or mesenchymal stem cells are considerably more homogeneous than sperm samples from multiple donors; an example of a biological system with less variability and experimental results are reproducible [142, 146]. I hypothesize that in a homogeneous biological system ANN would be superior to GPR.

3.4.2 Optimal Media Composition

My second objective was to couple the optimal theoretical model and empirical testing to optimize cryopreservation media composition for improved post-thaw motility in bovine sperm. I successfully coupled a Gaussian process regression and differential evolution to optimize the cryopreservation media composition by producing media that was comparable to traditional commercial media. The post-thaw motility in sperm cryopreserved in the optimized media were similar to commercial media. It took 72 trials over 9 generations using my methodology to generate media that was comparable to commercial, where as, a traditional approach, such as central composite design would have required at least 178 trials [61]. Moreover, my methodology has many advantages that traditional methods do not: (1) adaptation to new samples, (2) ability to add/subtract ingredients easily, (3) specify for "bad" freezers.

Traditional sperm cryopreservation media optimization often does not account for sample variation. Many studies apply an exhaustive search for the optimal CPM composition to the same sample population [12, 33, 170]. The optimal media that emerges is then optimized for the animals used in that study and same level of performance may differ on a different set of animals. With my methodology, only media that had high post-thaw motility move on for further validation. This approach eliminates the need to test every candidate media on the all available bulls which would be both time and resource intensive. Furthermore, my methodology is a general optimization approach that accounts for interactions of all components simultaneously, therefore it can be applied to other species, as well as, optimizing other types of media.

During the optimization process, one of the generated media compositions contained zero fructose. Fructose is often found in bull sperm cryopreservation media [16, 33, 92, 98] and is used as an energy source for the sperm post-thaw [5, 177]. The fructose free media still produced post-thaw motility that was still good. To my knowledge, it is unknown if trehalose can be used as an energy source for bovine sperm. Differential evolution is able to reduce the number of media components during the optimization. During the mutation/cross over stage, there is a chance that a component could be set to zero. If removing a component produces favourable results, in this case, good post-thaw motility, then it will persist into future generations. Being able to reduce unnecessary or redundant media components is essential, especially when optimization media with a large number of components.

Regardless of pre-freeze sperm parameters some sperm samples will freeze better than others [173]. Sperm donors can be classified as good or bad freezers depending on the sperm samples' ability to survive freezing with minimal cryopreservation damage [16]. Sperm samples that had high post-thaw motility cryopreserved with commercial media had similar results when cryopreserved with media generated by DE. However, some sperm frozen with commercial media had post-thaw motility around 40%, where as post-thaw motility increased to 50 - 60% when cryopreserved using media generated by DE (Figure 3.6). This would suggest that the media generated by DE is providing additional aid or protection to the sperm when being cryopreserved. A 10% increase in post-thaw motility could turn potential rejected sperm samples into accepted samples [37, 186]. Moreover, using my methodology optimized media can be created for just bad freezers. To do this, only sperm samples from bad freezers are needed and the algorithm will optimize the media for post-thaw motility.

Differential evolution and the inter and intra sperm sample variation does not guarantee improvement at each generation. Mean post-thaw motility from generations 1 - 4 increased each generation. However, from generation 4 to generation 5 the mean post-thaw motility decreased, then it improved at generation 6. This could have been caused by the new experimental media, the bulls selected simply performed poorly with the experimental media, or both. To wit, in generation 9 the variance had increased due to poor performance on half of the experimental media and a single bull with poor post-thaw motility. This may suggests that inter bull variation plays a larger part in the increased variance, as well as variations in media compositions.

Convergence indicates differential evolution is approaching an optimal, meaning generational improvement will begin to plateau. After coupling GPR and DE at generation 6 it took two more generations before the algorithm began to converge. At generation 8 (Figure 3.7) the algorithm the post-thaw motility began to plateau. The convergence rate of 2 - 4 generations has been previously reported [83, 142, 146]. As such a few more generations where average post-thaw motility has not improved significantly will be required to ensure that the algorithm has converged to a set of optimal cryopreservation media candidates. Once the algorithm has converged the optimal media candidates that had the highest post-thaw motility can be selected for further testing.

From these results the overall optimization could be adopted by industry for improving cryopreservation media composition and post-thaw motility of sperm. The media generated through this approach has results matching commercial media that has been highly optimized already. Future adaptions are promising and should be considered for other cell types and species.

4 General Discussion

4.1 Overall Significance of Research

Cryopreservation of genetic material and tissues has provided immense benefits, however, functionality and viability are reduced in tissues following the cryopreservation process. Towards improving post-thaw functionality and viability, I implemented tools that optimized the cryopreservation of bovine gametes and embryos, through reducing osmotic stress and cytotoxicity. For osmotic stress, I built tools to enable the optimization of the equilibration of CPAs such that the process is isochoric (constant volume) for bovine oocytes and embryos in order to reduce the effect of osmotic stress. I used numerical analysis techniques and physical manipulation of fluid delivery systems to monitor and respond to cell volume changes of oocytes and embryos during CPA addition. The techniques were developed to respond to each tissue that underwent CPA equilibration to facilitate optimized isochoric CPA equilibration at an individual sample level. The final microfluidic device successfully controlled delivery of CPAs and the approximated level-set method estimated cell volume as accurately as manual estimation.

For cytotoxicity, I optimized the composition of cryopreservation media (CPM; including CPAs) added to the cryopreservation protocol of bovine sperm in order to reduce cytotoxicity and maximize post-thaw motility. I used novel machine learning and mathematical algorithms to enhance previous approaches to optimize freezing media composition. This approach not only optimized the media components, but also created a new method for optimization of media composition. During the optimization process, I discovered that the Gaussian process regression model was ideal for predicting post-thaw motility of sperm cryopreserved with media generated by differential evolution. I was able to generate cryopreservation media over several months that performed similarly to industrial cryopreservation media, media which had been optimized over decades. These tools are the first steps towards improving post-thaw functionality and viability for new, less developed systems, as well as, improving on existing systems of assisted reproductive technology.

4.2 Limitations

I identified several limitations that may have affected the results of my research: (1) boundary leakage, (2) sample size, (3) limited optimization metrics, and (4) model used in data generation. In the image analysis of oocytes and embryos, the colour-based algorithm used edge information to find the tissue boundary which is susceptible to boundary leaking. Boundary leaking is when edges at the object boundary have low contrast or

there are gaps in the boundary causing the contour to leak out. This causes poor segmentation performance, which can be seen in the Hausdorff distance as the fitted ellipse was larger then the embryo itself. Boundary leaking provides an explanation for the variation seen in the Hausdorff distance. To address boundary leakage, the edge-based boundary detector should be replaced with a region-based boundary detector [157, 194] or region-based information should be combined with the edge-based information [174]. Region-based boundary detectors define the object boundary using the region statistical information (e.g. colour and texture). As such, the region-based information effectively makes low contrast boundaries irrelevant when computing the object boundary. This also makes region-based information less susceptible to image noise when finding the object boundary. Combining region and edge information together provides accurate and robust segmentation against low contrast boundary and image noise [174]. The edge-based information can be used to move the contour to the object boundary and region-based can control contour contraction or expansion [174]. The region and edge-based approach combines ease of edge-based algorithms with the

Small sample size was a limitation for the media optimization process. The comparison between my media and commercial media at generation 9 was on a small number of bulls ($n = 6$). The results provide strong evidence to undergo large scale trials, but at present no single cryopreservation medium can be selected as the optimal cryopreservation medium. The small sample size (8 trials per generation) impacts variation in media compositions. As the differential evolution algorithm converged so did the Gaussian process regression model. In particular, the trained model could discourage exploration of media compositions that are predicted to have low post-thaw motility. Even though my process has produced media that is comparable to commercial, it is possible that media compositions that surpass commercial could have been missed.

I used post-thaw motility as a measure of success for varying cryopreservation media protocols as it was an easy and inexpensive approach to evaluating post-thaw fertility. It also incorporates post-thaw functionality and viability together into one metric [60, 166]. However, using motility alone as a metric for measuring post-thaw viability and functionality may not provide a full picture of optimizing cryopreservation protocol. Gliozzi et al. [66] and Kumaresan et al. [93] showed that incorporating other kinetic factors (e.g. straight line velocity or ratio of sperm swimming linearly versus not linearly) should be accounted for when predicting post-thaw fertility. A better optimization metric could be a combination of kinetic factors including post-thaw motility.

As GPR was involved in data generation after generation 6, this may have biased the comparison between ANN, GPR, and experimental results towards GPR. From generation 1 to 6 both models were being trained on unbiased data, as DE used a pseudorandom number generator to select CPM trials. This random selection process would allow for an unbiased comparison between the models. However, from generation 7 on wards GPR was used to select CPM trials. Therefore, when the GPR model was updated with new experimental results, the adjustments to the previously approximated mean and covariance could have been small. Whereas, updating the ANN could have led to large changes in the approximated model. Furthermore, ANN and GPR were trained using all data from generations but only compared using generation 9, this also could

have skewed the comparison between ANN, GPR, and experimental results towards GPR. Instead of using post-thaw motility predictions on data from the training dataset, a new generation of CPM trials, generation 10, and its corresponding post-thaw motility data would be required. Then a comparison between ANN and GPR post-thaw motility predictions and experimental post-thaw motility would demonstrate which machine learning model offers a more precise estimation of theoretical post-thaw motility.

4.3 Future Directions

The tools that I have implemented were designed to reduce cytotoxicity and osmotic stress of cryopreserved bovine gametes and embryos. These tools can be used to tailor cryopreservation protocols at the individual level. As there is cell to cell variability in osmotic response [95], using the volumetric optimal approach adjusts CPA concentrations to changes in cell volume dynamically. Using this type of approach would not only minimize osmotic stress, but it would also eliminate the need to find cell membrane parameters. The volumetric approach uses cell volume estimates as input to the feedback control system, estimates of cell membrane parameters is encapsulated by the feedback control system. The media optimization approach can also be used to create cryopreservation media optimized for each individual. Individual cryopreservation media and post-thaw motility data pairs would be used to train the Gaussian process regression model. Then the differential evolution process would propose media that maximized post-thaw motility based on predictions from the model. Then sperm from the individual would be cryopreserved using new proposed media and the resulting post-thaw motility data would be used to update the individual-based model. Furthermore, the volumetric optimal approach and the media optimization approach could be combined to minimize both cytotoxicity and osmotic stress simultaneously.

Optimization of the cryopreservation protocol also needs to include cooling rates. The volumetric optimal approach would be able to dynamically compensate for changes in temperatures as CPA concentrations are dependent on cell volumes and adding cooling rate to the media optimization algorithm is as simple as adding it as a variable. In particular, coupling the volumetric optimal approach with a controlled rate freezer could allow for a fully automated liquidus tracking. Liquidus tracking is when a sample is frozen without ice formation due to high concentration of CPA. Cryopreotective agents are added incrementally such that as the temperature drops the CPA concentration matches the melting point of ice, this ensures that no ice is nucleated during the cryopreservation process while introducing high concentration of CPA at a low enough temperature that minimizes CPA toxicity. Optimal media composition is effected by cooling rates [146] and cell membrane parameters are also temperature dependent [1]. Including cooling rates as input to the media optimization algorithm is a simple process. By modifying data from existing cryopreservation protocols by taking the cryopreservation media composition and appending cooling rates at the end, creating a new dataset that can be used as input for the media optimization algorithm. This could improve post-thaw viability and functionality of new, less developed and well developed systems.

The optimization of new, less developed systems include cryopreservation of genetic materials from endangered species. An important consideration is maintaining genetic biodiversity for conservation purposes. For instance, cryopreserved gametes of endangered species can be used for captive breeding [56]. Captive breeding is a conservation approach that breeds animals in a controlled environment. Both of my tools can be applied to optimized gamete cryopreservation for endangered species. As oocytes and embryos be cryopreserved using the volumetric approach and the cryopreservation media optimized using the media optimization approach. Furthermore, cryopreserved somatic cells (any cell in the body except for reproductive cells, e.g. blood) hold enough genetic information where a genetic rescue program (e.g. cloning) can be used to save endangered species [178]. Therefore, the cryopreservation of somatic cells can optimized using the volumetric approach to equilibrate cells with CPAs and media optimization to create the optimal cryopreservation media.

4.4 Broader Relevance

My methodology can easily be adapted to optimizing the cryopreservation of other species. Optimizing the cryopreservation protocols for human gametes and embryos could be developed using both tools concurrently to improve post-thaw functionality and viability for people who want or require gamete or embryo cryopreservation. For oocytes and embryos combining the volumetric optimal approach and media optimization approach would minimize osmotic stress and cytotoxicity simultaneously. While human sperm cryopreservation would be optimized using the media optimization algorithm.

Cryopreservation protocols for tissues and organs could also be optimized. Tissue slices could be monitored using my image analysis software and media could be iteratively refined over time using the media optimization algorithm. As my media optimization approach does not restrict the number of components that can be simultaneously optimized, once an optimized media has been discovered, interactions between components could then be explored further. To optimize organ cryopreservation, the cryopreservation protocol (e.g. CPA concentration, cooling rate, and warming rate) could be used as input into the media optimization algorithm. Post-thaw viability and functionality results would be used to build a organ-based machine learning model. Then organs are cryopreserved and the protocol is iterative optimized until a cryopresrvation protocol emerges with a organ that is viable and functional post-thaw.

Simple modifications could allow the image analysis software to do simple object detection, such as when a new object enters a frame. My media optimization approach can also be deployed to optimize problem in other industries. Plastic injection molding process has multiple parameters to optimize and a similar approach has been shown to be successful [83, 198]. The chemistry of hard magnetic alloys have been optimized using a similar approach as well [87]. In short, the tools that I developed have applications that are not limited to cryobiology.

References

[1] Agca, Y., Liu, J., Critser, E. S., McGrath, J. J., and Critser, J. K. (1999). Temperature-dependent osmotic behavior of germinal vesicle and metaphase II stage bovine oocytes in the presence of Me2SO in relationship to cryobiology. *Molecular Reproduction and Development: Incorporating Gamete Research*, 53(1):59–67.

[2] Agca, Y., Liu, J., Peter, A. T., Critser, E. S., and Critser, J. K. (1998). Effect of developmental stage on bovine oocyte plasma membrane water and cryoprotectant permeability characteristics. *Molecular Reproduction and Development*, 49(4):408–415.

[3] Agca, Y., Liu, J., Rutledge, J. J., Critser, E. S., and Critser, J. K. (2000). Effect of osmotic stress on the developmental competence of germinal vesicle and metaphase II stage bovine cumulus oocyte complexes and its relevance to cryopreservation. *Molecular Reproduction and Development*, 55(2):212–219.

[4] Aman, R. R. and Parks, J. E. (1994). Effects of cooling and rewarming on the meiotic spindle and chromosomes of in vitro-matured bovine oocytes. *Biology of reproduction*, 50(1):103–110.

[5] Amirat, L., Anton, M., Tainturier, D., Chatagnon, G., Battut, I., and Courtens, J. L. (2005). Modifications of bull spermatozoa induced by three extenders: Biociphos, low density lipoprotein and Triladyl, before, during and after freezing and thawing. *Reproduction*, 129(4):535–543.

[6] Anchordoguy, T. J., Rudolph, A. S., Carpenter, J. F., and Crowe, J. H. (1987). Modes of interaction of cryoprotectants with membrane phospholipids during freezing. *Cryobiology*, 24(4):324–331.

[7] Angermueller, C., Pärnamaa, T., Parts, L., and Stegle, O. (2016). Deep learning for computational biology. *Molecular Systems Biology*, 12(7):878.

[8] Arav, A., Zeron, Y., Leslie, S. B., Behboodi, E., Anderson, G. B., and Crowe, J. H. (1996). Phase Transition Temperature and Chilling Sensitivity of Bovine Oocytes. *Cryobiology*, 33(6):589–599.

[9] Argyle, C. E., Harper, J. C., and Davies, M. C. (2016). Oocyte cryopreservation: where are we now? *Human Reproduction Update*, 22(4):440–449.

[10] Ashrafi, I., Kohram, H., and Ardabili, F. F. (2013). Antioxidative effects of melatonin on kinetics, microscopic and oxidative parameters of cryopreserved bull spermatozoa. *Animal Reproduction Science*, 139(1-4):25–30.

[11] Assumpção, M., Milazzotto, M. P., Simões, R., Nicacio, A. C., Mendes, C. M., Mello, M. R. B., and Visintin, J. A. (2008). In vitro survival of in vitro-produced bovine embryos cryopreserved by slow freezing, fast freezing and vitrification. *Animal Reproduction (AR)*, 5(3):116–120.

[12] Awad, M. M. (2011). Effect of some permeating cryoprotectants on CASA motility results in cryopreserved bull spermatozoa. *Animal Reproduction Science*, 123(3-4):157–162.

[13] Ba, D. and Boyaci, I. H. (2007). Modeling and optimization II: Comparison of estimation capabilities of response surface methodology with artificial neural networks in a biochemical reaction. *Journal of Food Engineering*, 78(3):846–854.

[14] Bailey, J. L., Bilodeau, J. F., and Cormier, N. (2000). Semen cryopreservation in domestic animals: a damaging and capacitating phenomenon. *Journal of andrology*, 21(1):1–7.

[15] Balasubramanian, S. and Rho, G. J. (2006). Effect of chilling on the development of in vitro produced bovine embryos at various cleavage stages. *Journal of Assisted Reproduction and Genetics*, 23(2):55–61.

[16] Barbas, J. P. and Mascarenhas, R. D. (2009). Cryopreservation of domestic animal sperm cells. *Cell and Tissue Banking*, 10(1):49–62.

[17] Barnes, B. M. (1989). Freeze avoidance in a mammal: Body temperatures below 0°C in an arctic hibernator. *Science*, 244(4912):1593–1595.

[18] Baust, J. M. (2002). Molecular Mechanisms of Cellular Demise Associated with Cryopreservation Failure. *Cell Preservation Technology*, 1(1):17–31.

[19] Belonoschkin, B. (1956). The science of reproduction and its traditions. *Int J Fertil*, 1(215):24.

[20] Benham, H. M., McCollum, M. P., Nol, P., Frey, R. K., Clarke, P. R., Rhyan, J. C., and Barfield, J. P. (2021). Production of embryos and a live offspring using post mortem reproductive material from bison (Bison bison bison) originating in Yellowstone National Park, USA. *Theriogenology*, 160:33–39.

[21] Benson, J. D., Chicone, C. C., and Critser, J. K. (2011). A general model for the dynamics of cell volume, global stability, and optimal control. *Journal of Mathematical Biology*, 63(2):339–359.

[22] Benson, J. D., Chicone, C. C., and Critser, J. K. (2012a). Analytical Optimal Controls for the State Constrained Addition and Removal of Cryoprotective Agents. *Bulletin of Mathematical Biology*, 74(7):1516–1530.

[23] Benson, J. D., Higgins, A. Z., Desai, K., and Eroglu, A. (2018). A toxicity cost function approach to optimal CPA equilibration in tissues. *Cryobiology*, 80:144–155.

[24] Benson, J. D., Woods, E. J., Walters, E. M., and Critser, J. K. (2012b). The cryobiology of spermatozoa. *Theriogenology*, 78(8):1682–1699.

[25] Best, B. P. (2015). Cryoprotectant Toxicity: Facts, Issues, and Questions. *Rejuvenation Research*, 18(5):422–436.

[26] Betz, G. C. M. (2007). Using the rate of genetic change and the population structure of cattle to better target genetic progress. In *Proceedings of 39th beef improvement federation symposium, Fort Collins, CO*, pages 103–109.

[27] Bhat, M. H., Blondin, P., Vincent, P., and Benson, J. D. (2020). Low concentrations of 3-O-methylglucose improve post thaw recovery in cryopreserved bovine spermatozoa. *Cryobiology*, 95(April):15–19.

[28] Bissoyi, A., Nayak, B., Pramanik, K., and Sarangi, S. K. (2014). Targeting cryopreservation-induced cell death: A review. *Biopreservation and Biobanking*, 12(1):23–34.

[29] Bó, G. and Mapletoft, R. (2013). Evaluation and classification of bovine embryos. *Animal Reproduction*, 10(3):344–348.

[30] Bradski, G. (2000). The OpenCV Library. *Dr. Dobb's Journal of Software Tools*.

[31] Bulat, I. and Lei, X. (2017). Segmentation of organs-at-risks in head and neck CT images using convolutional neural networks. *Medical Physics*, 44(2):547–557.

[32] Chang, M. C. (1959). Fertilization of Rabbit Ova in vitro. *Nature*, 184(4684):466–467.

[33] Chaveiro, A., Machado, L., Frijters, A., Engel, B., and Woelders, H. (2006). Improvement of parameters of freezing medium and freezing protocol for bull sperm using two osmotic supports. *Theriogenology*, 65(9):1875–1890.

[34] Chen, S. U., Lien, Y. R., Chao, K. H., Ho, H. N., Yang, Y. S., and Lee, T. Y. (2003). Effects of cryopreservation on meiotic spindles of oocytes and its dynamics after thawing: Clinical implications in oocyte freezing - A review article. *Molecular and Cellular Endocrinology*, 202(1-2):101–107.

[35] Chen, Y., Foote, R. H., and Brockett, C. C. (1993). Effect of sucrose, trehalose, hypotaurine, taurine, and blood serum on survival of frozen bull sperm. *Cryobiology*, 30(4):423–431.

[36] Chiu, Y. H., Edifor, R., Rosner, B. A., Nassan, F. L., Gaskins, A. J., Mínguez-Alarcón, L., Williams, P. L., Tanrikut, C., Hauser, R., and Chavarro, J. E. (2017). What Does a Single Semen Sample Tell You? Implications for Male Factor Infertility Research. *American Journal of Epidemiology*, 186(8):918–926.

[37] Cooper, T. G., Noonan, E., von Eckardstein, S., Auger, J., Baker, H. W., Behre, H. M., Haugen, T. B., Kruger, T., Wang, C., Mbizvo, M. T., and Vogelsong, K. M. (2009). World Health Organization reference values for human semen characteristics. *Human Reproduction Update*, 16(3):231–245.

[38] Crowe, J. H., Carpenter, J. F., and Crowe, L. M. (1998). the Role of Vitrification in Anhydrobiosis. *Annual Review of Physiology*, 60(1):73–103.

[39] Davidson, A. F., Benson, J. D., and Higgins, A. Z. (2014). Mathematically optimized cryoprotectant equilibration procedures for cryopreservation of human oocytes. *Theoretical Biology and Medical Modelling*, 11(1):1–19.

[40] Davidson, A. F., Glasscock, C., McClanahan, D. R., Benson, J. D., and Higgins, A. Z. (2015). Toxicity Minimized Cryoprotectant Addition and Removal Procedures for Adherent Endothelial Cells. *PLoS ONE*, 10(11):1–22.

[41] DeLong, J. P., Gibert, J. P., Luhring, T. M., Bachman, G., Reed, B., Neyer, A., and Montooth, K. L. (2017). The combined effects of reactant kinetics and enzyme stability explain the temperature dependence of metabolic rates. *Ecology and Evolution*, 7(11):3940–3950.

[42] Desai, K. M., Survase, S. A., Saudagar, P. S., Lele, S. S., and Singhal, R. S. (2008). Comparison of artificial neural network (ANN) and response surface methodology (RSM) in fermentation media optimization: Case study of fermentative production of scleroglucan. *Biochemical Engineering Journal*, 41(3):266–273.

[43] Devireddy, R. V., Swanlund, D. J., Roberts, K. P., and Bischof, J. C. (1999). Subzero Water Permeability Parameters of Mouse Spermatozoa in the Presence of Extracellular Ice and Cryoprotective Agents1. *Biology of Reproduction*, 61(3):764–775.

[44] Dong, Q., Hill, D., and VandeVoort, C. A. (2009). Interactions among pre-cooling, cryoprotectant, cooling, and thawing for sperm cryopreservation in rhesus monkeys. *Cryobiology*, 59(3):268–274.

[45] Donnelly, E. T. (2001). Assessment of DNA integrity and morphology of ejaculated spermatozoa from fertile and infertile men before and after cryopreservation. *Human Reproduction*, 16(6):1191–1199.

[46] Elliott, J. A. (2010). Introduction to the special issue: Thermodynamic aspects of cryobiology. *Cryobiology*, 60(1):1–3.

[47] Elmoazzen, H. Y., Poovadan, A., Law, G. K., Elliott, J. A. W., McGann, L. E., and Jomha, N. M. (2007). Dimethyl sulfoxide toxicity kinetics in intact articular cartilage. *Cell and tissue banking*, 8(2):125–133.

[48] et. all. Hastie, T. (2009). Springer Series in Statistics The Elements of Statistical Learning. *The Mathematical Intelligencer*, 27(2):83–85.

[49] Fahy, G. M., MacFarlane, D. R., Angell, C. A., and Meryman, H. T. (1984). Vitrification as an approach to cryopreservation. *Cryobiology*, 21(4):407–426.

[50] Fahy, G. M., Wowk, B., Wu, J., and Paynter, S. (2004). Improved vitrification solutions based on the predictability of vitrification solution toxicity. *Cryobiology*, 48(1):22–35.

[51] Fang, C., Ji, F., Shu, Z., and Gao, D. (2017). Determination of the temperature-dependent cell membrane permeabilities using microfluidics with integrated flow and temperature control. *Lab on a Chip*, 17(5):951–960.

[52] Fatehi, A. N., Bevers, M. M., Schoevers, E., Roelen, B. A., Colenbrander, B., and Gadella, B. M. (2006). DNA damage in bovine sperm does not block fertilization and early embryonic development but induces apoptosis after the first cleavages. *Journal of Andrology*, 27(2):176–188.

[53] Feng, W. and Yang, S. (2016). Thermomechanical processing optimization for 304 austenitic stainless steel using artificial neural network and genetic algorithm. *Applied Physics A*, 122(12):1–10.

[54] Fiser, P. S. and Fairfull, R. W. (1986). The effects of rapid cooling (cold shock) of ram semen, photoperiod, and egg yolk in diluents on the survival of spermatozoa before and after freezing. *Cryobiology*, 23(6):518–524.

[55] Fletcher, G. L., Hew, C. L., and Davies, P. L. (2001). Antifreeze proteins of teleost fishes.

[56] Fraser, D. J. (2008). How well can captive breeding programs conserve biodiversity? A review of salmonids. *Evolutionary Applications*, 1(4):535–586.

[57] Fuller, B. and Paynter, S. (2004). Fundamentals of cryobiology in reproductive medicine. *Reproductive BioMedicine Online*, 9(6):680–691.

[58] Fuller, B. J. (2004). Cryoprotectants: the essential antifreezes to protect life in the frozen state. 25(6):375–388.

[59] Fuller, B. J., Lane, N., and Benson, E. E. (2004). *Life in the frozen state*. CRC Press, Boca Raton.

[60] Gadea, J. (2005). Sperm factors related to in vitro and in vivo porcine fertility. *Theriogenology*, 63(2 SPEC. ISS.):431–444.

[61] Galbraith, S. C., Bhatia, H., Liu, H., and Yoon, S. (2018). Media formulation optimization: current and future opportunities. *Current Opinion in Chemical Engineering*, 22:42–47.

[62] Gallardo, M., Saenz, J., and Risco, R. (2019). Human oocytes and zygotes are ready for ultra-fast vitrification after 2 minutes of exposure to standard CPA solutions. *Scientific Reports*, 9(1):1–9.

[63] Gao, D. Y., Ashworth, E., Watson, P. F., Kleinhans, F. W., Mazur, P., and Critser, J. K. (1993). Hyperosmotic tolerance of human spermatozoa: Separate effects of glycerol, sodium chloride, and sucrose on spermolysis. *Biology of Reproduction*, 49(1):112–123.

[64] Gao, D. Y., Liu, J., Liu, C., Mcgann, L. E., Watson, P. F., Kleinhans, F. W., Mazur, P., Critser, E. S., and Critser, J. K. (1995). Andrology: Prevention of osmotic injury to human spermatozoa during addition and removal of glycerol. *Human Reproduction*, 10(5):1109–1122.

[65] George, M. A. and Johnson, M. H. (1993). Use of fetal bovine serum substitutes for the protection of the mouse zona pellucida against hardening during cryoprotectant addition. *Human reproduction (Oxford, England)*, 8(11):1898–1900.

[66] Gliozzi, T. M., Turri, F., Manes, S., Cassinelli, C., and Pizzi, F. (2017). The combination of kinetic and flow cytometric semen parameters as a tool to predict fertility in cryopreserved bull semen. *Animal*, 11(11):1975–1982.

[67] Goodfellow, I., Bengio, Y., and Courville, A. (2016). *Deep Learning*. Adaptive Computation and Machine Learning series. MIT Press.

[68] Grötter, L. G., Cattaneo, L., Marini, P. E., Kjelland, M. E., and Ferré, L. B. (2019). Recent advances in bovine sperm cryopreservation techniques with a focus on sperm post-thaw quality optimization. *Reproduction in Domestic Animals*, 54(4):655–665.

[69] Gulyanon, W., Morand, C., Robertson, N. M., and Wallace, A. M. (2011). Real-time active visual tracking with level sets. *4th International Conference on Imaging for Crime Detection and Prevention 2011 (ICDP 2011)*, pages P25–P25.

[70] Gunasena, K. T. and Critser, J. K. (1997). Utility of viable tissues ex vivo: banking of reproductive cells and tissues. In *Reproductive Tissue Banking*, pages 1–21. Elsevier.

[71] Gürler, H., Malama, E., Heppelmann, M., Calisici, O., Leiding, C., Kastelic, J. P., and Bollwein, H. (2015). Effects of cryopreservation on sperm viability, synthesis of reactive oxygen species, and DNA damage of bovine sperm. *Theriogenology*, 86(2):562–571.

[72] Hagiwara, M., Choi, J. H., Devireddy, R. V., Roberts, K. P., Wolkers, W. F., Makhlouf, A., and Bischof, J. C. (2009). Cellular Biophysics During Freezing of Rat and Mouse Sperm Predicts Post-thaw Motility1. *Biology of Reproduction*, 81(4):700–706.

[73] Han, L., Pu, T., Wang, X., Liu, B., Wang, Y., Feng, J., and Zhang, X. (2018). Optimization of a protective medium for enhancing the viability of freeze-dried Bacillus amyloliquefaciens B1408 based on response surface methodology. *Cryobiology*, 81(February):101–106.

[74] Hansen, P. J. and Block, J. (2004). Towards an embryocentric world: The current and potential uses of embryo technologies in dairy production. *Reproduction, Fertility and Development*, 16(1-2):1–14.

[75] Harris, D. L. and Newman, S. (1994). Breeding for profit: synergism between genetic improvement and livestock production (a review). *Journal of Animal Science*, 72(8):2178–2200.

[76] Heo, Y. S., Lee, H. J., Hassell, B. A., Irimia, D., Toth, T. L., Elmoazzen, H., and Toner, M. (2011). Controlled loading of cryoprotectants (CPAs) to oocyte with linear and complex CPA profiles on a microfluidic platform. *Lab on a Chip*, 11(20):3530–3537.

[77] Hezavehei, M., Sharafi, M., Kouchesfahani, H. M., Henkel, R., Agarwal, A., Esmaeili, V., and Shahverdi, A. (2018). Sperm cryopreservation: A review on current molecular cryobiology and advanced approaches. *Reproductive BioMedicine Online*, 37(3):327–339.

[78] Ho, C. M. B., Ng, S. H., Li, K. H. H., and Yoon, Y. J. (2015). 3D printed microfluidics for biological applications. *Lab on a Chip*, 15(18):3627–3637.

[79] Holt, W. V. (2000). Basic aspects of frozen storage of semen. *Animal Reproduction Science*, 62(1-3):3–22.

[80] Holt, W. V., Medrano, A., Thurston, L. M., and Watson, P. F. (2005). The significance of cooling rates and animal variability for boar sperm cryopreservation: Insights from the cryomicroscope. *Theriogenology*, 63(2 SPEC. ISS.):370–382.

[81] Hu, T.-x., Zhu, H.-b., Sun, W.-j., Hao, H.-s., Zhao, X.-m., Du, W.-h., and Wang, Z.-l. (2016). Sperm pretreatment with glutathione improves IVF embryos development through increasing the viability and antioxidative capacity of sex-sorted and unsorted bull semen. *Journal of Integrative Agriculture*, 15(10):2326–2335.

[82] Hua, S. Z. and Pennell, T. (2009). A microfluidic chip for real-time studies of the volume of single cells. *Lab on a Chip*, 9(2):251–256.

[83] Huang, H. X., Li, J. C., and Xiao, C. L. (2015). A proposed iteration optimization approach integrating backpropagation neural network with genetic algorithm. *Expert Systems with Applications*, 42(1):146–155.

[84] Hwang, I. S. and Hochi, S. (2014). Recent progress in cryopreservation of bovine oocytes. *BioMed Research International*, 2014.

[85] Jacobs, M. H. (1933). The simultaneous measurement of cell permeability to water and to dissolved substances. *Journal of Cellular and Comparative Physiology*, 2(4):427–444.

[86] Jacobs, M. H. and Stewart, D. R. (1932). A simple method for the quantitative measurement of cell permeability. *Journal of Cellular and Comparative Physiology*, 1(1):71–82.

[87] Jha, R., Dulikravich, G. S., Chakraborti, N., Fan, M., Schwartz, J., Koch, C. C., Colaco, M. J., Poloni, C., and Egorov, I. N. (2016). Algorithms for design optimization of chemistry of hard magnetic alloys using experimental data. *Journal of Alloys and Compounds*, 682:454–467.

[88] Jomha, N. M., Weiss, A. D. H., Fraser Forbes, J., Law, G. K., Elliott, J. A. W., and McGann, L. E. (2010). Cryoprotectant agent toxicity in porcine articular chondrocytes. *Cryobiology*, 61(3):297–302.

[89] Kamel, R. M. (2013). Assisted reproductive technology after the birth of Louise Brown. *Journal of Reproduction and Infertility*, 14(3):96–109.

[90] Karlsson, J. O. M., Szurek, E. A., Higgins, A. Z., Lee, S. R., and Eroglu, A. (2014). Optimization of cryoprotectant loading into murine and human oocytes. *Cryobiology*, 68(1):18–28.

[91] Kedem, O. and Katchalsky, A. (1958). Thermodynamic analysis of the permeability of biological membranes to non-electrolytes. *BBA - Biochimica et Biophysica Acta*, 27(C):229–246.

[92] Khalil, W. A., El-Harairy, M. A., Zeidan, A. E., Hassan, M. A., and Mohey-Elsaeed, O. (2018). Evaluation of bull spermatozoa during and after cryopreservation: Structural and ultrastructural insights. *International Journal of Veterinary Science and Medicine*, 6:S49–S56.

[93] Kumaresan, A., Johannisson, A., Al-Essawe, E. M., and Morrell, J. M. (2017). Sperm viability, reactive oxygen species, and DNA fragmentation index combined can discriminate between above- and below-average fertility bulls. *Journal of Dairy Science*, 100(7):5824–5836.

[94] Lahmann, J. M., Benson, J. D., and Higgins, A. Z. (2018). Concentration dependence of the cell membrane permeability to cryoprotectant and water and implications for design of methods for post-thaw washing of human erythrocytes. *Cryobiology*, 80:1–11.

[95] Lahmann, J. M., Sanchez, C. C., Benson, J. D., Acker, J. P., and Higgins, A. Z. (2020). Implications of variability in cell membrane permeability for design of methods to remove glycerol from frozen-thawed erythrocytes. *Cryobiology*, 92:168–179.

[96] Lamb, G. C. and DiLorenzo, N. (2013). *Current and future reproductive technologies and world food production*, volume 752. Springer.

[97] Lawson, A., Ahmad, H., and Sambanis, A. (2011). Cytotoxicity effects of cryoprotectants as single-component and cocktail vitrification solutions. *Cryobiology*, 62(2):115–122.

[98] Leeuw, F. E. D., Leeuw, A. M. D., Daas, J. H. G. D., Colenbrander, B., and Verkleij, A. J. (1993). Effects of Various Cryoprotective Agents and Membrane-Stabilizing Compounds on Bull Sperm Membrane Integrity after Cooling and Freezing. *Cryobiology*, 30(1):32–44.

[99] Leibo, S. P., Martio, A., Kobayashi, S., and Pollard, J. W. (1996). Stage-dependent sensitivity of oocytes and embryos to low temperatures. *Animal Reproduction Science*, 42(1-4):45–53.

[100] Levi-Setti, P. E., Patrizio, P., and Scaravelli, G. (2016). Evolution of human oocyte cryopreservation: Slow freezing versus vitrification. *Current Opinion in Endocrinology, Diabetes and Obesity*, 23(6):445–450.

[101] Levin, R. L. (1982). A generalized method for the minimization of cellular osmotic stresses and strains during the introduction and removal of permeable cryoprotectants. *Journal of Biomechanical Engineering*, 104(2):81–86.

[102] Levin, R. L. and Miller, T. W. (1981). An optimum method for the introduction or removal of permeable cryoprotectants: Isolated cells. *Cryobiology*, 18(1):32–48.

[103] Li, C., Xu, C., Gui, C., and Fox, M. D. (2010). Distance regularized level set evolution and its application to image segmentation. *IEEE Transactions on Image Processing*, 19(12):3243–3254.

[104] Li, Y., Wang, H., and Tingrui, P. (2013). Intracellular ice formation (IIF) during freeze-thaw repetitions. *International Journal of Heat and Mass Transfer*, 64:436–443.

[105] Liu, J., Mullen, S., Meng, Q., Critser, J., and Dinnyes, A. (2009). Determination of oocyte membrane permeability coefficients and their application to cryopreservation in a rabbit model. *Cryobiology*, 59(2):127–134.

[106] Liu, W., Zhao, G., Shu, Z., Wang, T., Zhu, K., and Gao, D. (2015). High-precision approach based on microfluidic perfusion chamber for quantitative analysis of biophysical properties of cell membrane. *International Journal of Heat and Mass Transfer*, 86:869–879.

[107] Loewke, N. O., Pai, S., Cordeiro, C., Black, D., King, B. L., Contag, C. H., Chen, B., Baer, T. M., and Solgaard, O. (2018). Automated Cell Segmentation for Quantitative Phase Microscopy. *IEEE Transactions on Medical Imaging*, 37(4):929–940.

[108] Love, C. C. (2011). Relationship between sperm motility, morphology and the fertility of stallions. *Theriogenology*, 76(3):547–557.

[109] Lovelock, J. E. (1954). The protective action of neutral solutes against haemolysis by freezing and thawing. *The Biochemical journal*, 56(2):265–270.

[110] Lu, Y., Huang, L., Yang, T., Lv, F., and Lu, Z. (2017). Optimization of a cryoprotective medium to increase the viability of freeze-dried Streptococcus thermophilus by response surface methodology. *LWT - Food Science and Technology*, 80:92–97.

[111] Lusianti, R. E., Benson, J. D., Acker, J. P., and Higgins, A. Z. (2013). Rapid removal of glycerol from frozen-thawed red blood cells. *Biotechnology Progress*, 29(3):609–620.

[112] Madabhushi, A. and Metaxas, D. N. (2003). Combining low-, high-level and empirical domain knowledge for automated segmentation of ultrasonic breast lesions. *IEEE Transactions on Medical Imaging*, 22(2):155–169.

[113] Mage, P. L., Ferguson, B. S., Maliniak, D., Ploense, K. L., Kippin, T. E., and Soh, H. T. (2017). Closed-loop control of circulating drug levels in live animals. *Nature Biomedical Engineering*, 1(5):1–10.

[114] Malama, E., Zeron, Y., Janett, F., Siuda, M., Roth, Z., and Bollwein, H. (2017). Use of computer-assisted sperm analysis and flow cytometry to detect seasonal variations of bovine semen quality. *Theriogenology*, 87:79–90.

[115] Malmo, J. (2011). Bull Management — Dairy Farms. pages 475–480. Academic Press, San Diego.

[116] Mandawala, A. A., Harvey, S. C., Roy, T. K., and Fowler, K. E. (2016). Cryopreservation of animal oocytes and embryos: Current progress and future prospects. *Theriogenology*, 86(7):1637–1644.

[117] Maroto-Morales, A., Ramón, M., García-Álvarez, O., Soler, A. J., Fernández-Santos, M. R., Roldan, E. R., Gomendio, M., Pérez-Guzmán, M. D., and Garde, J. J. (2012). Morphometrically-distinct sperm

subpopulations defined by a multistep statistical procedure in Ram ejaculates: Intra- and interindividual variation. *Theriogenology*, 77(8):1529–1539.

[118] Mayer, D. T. and Lasley, J. F. (1945). The Factor in Egg Yolk Affecting the Resistance, Storage Potentialities, and Fertilizing Capacity of Mammalian Spermatozoa. *Journal of Animal Science*, 4(3):261–269.

[119] Mazur, P. (1963). Kinetics of Water Loss From Cells At Subzero Temperatures and the Likelihood of Intracellular Freezing. *The Journal of general physiology*, 47:347–369.

[120] Mazur, P. (1965). The role of cell membranes in the freezing of yeast and other single cells. *Annals of the New York Academy of Sciences*, 125(2):658–676.

[121] Mazur, P. (1970). Cryobiology: The Freezing of Biological Systems. *Science*, 168(3934):939–949.

[122] Mazur, P. (1985). Basic concepts in freezing cells.

[123] Mazur, P., Rall, W. F., and Leibo, S. P. (1984). Kinetics of water loss and the likelihood of intracellular freezing in mouse ova - Influence of the method of calculating the temperature dependence of water permeability. *Cell Biophysics*, 6(3):197–213.

[124] Mbogba, M. K., Haider, Z., Hossain, S. M., Huang, D., Memon, K., Panhwar, F., Lei, Z., and Zhao, G. (2018). The application of convolution neural network based cell segmentation during cryopreservation. *Cryobiology*, (June):0–1.

[125] McKhann, H. I., Gery, C., Bérard, A., Lévêque, S., Zuther, E., Hincha, D. K., De Mita, S., Brunel, D., and Téoulé, E. (2008). Natural variation in CBF gene sequence, gene expression and freezing tolerance in the Versailles core collection of Arabidopsis thaliana. *BMC Plant Biology*, 8:1–18.

[126] Morschett, H., Freier, L., Rohde, J., Wiechert, W., Von Lieres, E., and Oldiges, M. (2017). A framework for accelerated phototrophic bioprocess development: Integration of parallelized microscale cultivation, laboratory automation and Kriging-assisted experimental design. *Biotechnology for Biofuels*, 10(1):1–13.

[127] Muldrew, K. and McGann, L. E. (1990). Mechanisms of intracellular ice formation. *Biophysical Journal*, 57(3):525–532.

[128] Mullen, S. F. and Critser, J. K. (2007). The science of cryobiology. *Cancer treatment and research*, 138:83.

[129] Mullen, S. F. and Fahy, G. M. (2012). A chronologic review of mature oocyte vitrification research in cattle, pigs, and sheep. *Theriogenology*, 78(8):1709–1719.

[130] Mullen, S. F., Li, M., Li, Y., Chen, Z. J., and Critser, J. K. (2008). Human oocyte vitrification: the permeability of metaphase II oocytes to water and ethylene glycol and the appliance toward vitrification. *Fertility and Sterility*, 89(6):1812–1825.

[131] Myers, R. H., Montgomery, D. C., and Anderson-Cook, C. M. (1996). *Response Surface Methodology: Process and Product Optimization Using Designed Experiments*, volume 38 of *Wiley series in probability and statistics*. Wiley, Hoboken, N.J., 3rd ed. / edition.

[132] Nagai, T., Yamaguchi, K., and Moriwaki, C. (1982). Studies on the effects of sugars on washed human sperm motility. *Journal of pharmacobio-dynamics*, 5(8):564–567.

[133] Nannou, T. K., Jouhara, H., Trembley, J., and Herrmann, J. (2016). Cryopreservation: Methods, equipment and critical concerns. *Refrigeration Science and Technology*, 22-25-June:247–258.

[134] Nocedal, J. and Wright, S. J. (2006). *Numericak Optimization*.

[135] Ogle, D. H., Wheeler, P., and Dinno, A. (2020). *FSA: Fisheries Stock Analysis*.

[136] Ombelet, W. and Van Robays, J. (2015). Artificial insemination history: hurdles and milestones. *Facts, views & vision in ObGyn*, 7(2):137–43.

[137] Pace, M. M. and Graham, E. F. (1974). Components in Egg Yolk which Protect Bovine Spermatozoa during Freezing. *Journal of Animal Science*, 39(6):1144–1149.

[138] Parks, J. E. and Graham, J. K. (1992). Effects of cryopreservation procedures on sperm membranes. *Theriogenology*, 38(2):209–222.

[139] Parrish, J. J., Susko-Parrish, J. L., Leibfried-Rutledge, M. L., Critser, E. S., Eyestone, W. H., and First, N. L. (1986). Bovine in vitro fertilization with frozen-thawed semen. *Theriogenology*, 25(4):591–600.

[140] Paynter, S. J. (2005). A rational approach to oocyte cryopreservation. *Reproductive BioMedicine Online*, 10(5):578–586.

[141] Pegg, D. E. (2007). Principles of cryopreservation. *Methods in molecular biology (Clifton, N.J.)*, 368:39–57.

[142] Pi, C.-H., Dosa, P. I., and Hubel, A. (2019). Differential Evolution for the Optimization of DMSO-free Cryoprotectants: Influence of Control Parameters. *Journal of Biomechanical Engineering*.

[143] Pickering, S. J., Braude, P. R., Johnson, M. H., Cant, A., and Currie, J. (1990). Transient cooling to room temperature can cause irreversible disruption of the meiotic spindle in the human oocyte. *Fertility and sterility*, 54(1):102–108.

[144] Polge, C., Smith, A. U., and Parkes, A. (1949). Revival of spermatozoa after vitrification and dehydration.

[145] Pollard, J. W. and Leibo, S. P. (1994). Chilling sensitivity of mammalian embryos. *Theriogenology*, 41(1):101–106.

[146] Pollock, K., Budenske, J. W., McKenna, D. H., Dosa, P. I., and Hubel, A. (2017). Algorithm-driven optimization of cryopreservation protocols for transfusion model cell types including Jurkat cells and mesenchymal stem cells. *Journal of Tissue Engineering and Regenerative Medicine*, 11(10):2806–2815.

[147] Prentice, J. R. and Anzar, M. (2011). Cryopreservation of mammalian oocyte for conservation of animal genetics. *Veterinary Medicine International*, 2011.

[148] Prewitt, J. M. S. (1970). Object enhancement and extraction. *Picture processing and Psychopictorics*, 10(1):15–19.

[149] Price, K. and Storn, R. (1997). Differential Evolution – A Simple and Efficient Heuristic for Global Optimization over Continuous Spaces. *Journal of Global Optimization*, (11):341–359.

[150] Purdy, P. H. (2006). A review on goat sperm cryopreservation. *Small Ruminant Research*, 63(3):215–225.

[151] Purdy, P. H. and Graham, J. K. (2004). Effect of cholesterol-loaded cyclodextrin on the cryosurvival of bull sperm. *Cryobiology*, 48(1):36–45.

[152] R Core Team (2020). *R: A Language and Environment for Statistical Computing*. R Foundation for Statistical Computing, Vienna, Austria.

[153] Raju, R., Höhn, H., Karnutsch, C., Khoshmanesh, K., and Bryant, G. (2019). Measuring volume kinetics of human monocytes in response to cryoprotectants using microfluidic technologies. *Applied Physics Letters*, 114(22).

[154] Rall, W. F. and Fahy, G. M. (1985). Ice-free cryopreservation of mouse embryos at -196 degrees C by vitrification. *Nature*, 313(6003):573–575.

[155] Rasmussen, C. E. and Williams, C. K. I. (2006). *Gaussian processes for machine learning*, volume 2. MIT press Cambridge, MA.

[156] Ruffing, N. A., Steponkus, P. L., Pitt, R. E., and Parks, J. E. (1993). Osmometric Behavior, Hydraulic Conductivity, and Incidence of Intracellular Ice Formation in Bovine Oocytes at Different Developmental Stages. *Cryobiology*, 30(6):562–580.

[157] Rusnell, B. J., Pierson, R. A., Singh, J., Adams, G. P., and Eramian, M. G. (2008). Level set segmentation of bovine corpora lutea in ex situ ovarian ultrasound images. *Reproductive Biology and Endocrinology*, 6:1–16.

[158] Sackmann, E. K., Fulton, A. L., and Beebe, D. J. (2014). The present and future role of microfluidics in biomedical research. *Nature*, 507(7491):181–189.

[159] Sadanandan, S. K., Ranefall, P., Le Guyader, S., and Wählby, C. (2017). Automated Training of Deep Convolutional Neural Networks for Cell Segmentation. *Scientific Reports*, 7(1):1–7.

[160] Saeednia, S., Bahadoran, H., Amidi, F., Asadi, M. H., Naji, M., Fallahi, P., and Nejad, N. A. (2015). Nerve growth factor in human semen: Effect of nerve growth factor on the normozoospermic men during cryopreservation process. *Iranian Journal of Basic Medical Sciences*, 18(3):292–299.

[161] Saragusty, J. and Arav, A. (2011). Current progress in oocyte and embryo cryopreservation by slow freezing and vitrification. *Reproduction*, 141(1):1–19.

[162] Selinummi, J., Seppälä, J., Yli-Harja, O., and Puhakka, J. A. (2005). Software for quantification of labeled bacteria from digital microscope images by automated image analysis. *BioTechniques*, 39(6):859–862.

[163] Shah, N., Singh, V., Yadav, H. P., Verma, M., Chauhan, D. S., Saxena, A., Yadav, S., and Swain, D. K. (2017). Effect of reduced glutathione supplementation in semen extender on tyrosine phosphorylation and apoptosis like changes in frozen thawed Hariana bull spermatozoa. *Animal Reproduction Science*, 182(March):111–122.

[164] Shi, Y. and Karl, W. C. (2008). A real-time algorithm for the approximation of level-set-based curve evolution. *IEEE Transactions on Image Processing*, 17(5):645–656.

[165] Sieme, H., Oldenhof, H., and Wolkers, W. F. (2016). Mode of action of cryoprotectants for sperm preservation. *Animal Reproduction Science*, 169:2–5.

[166] Simon, L. and Lewis, S. E. (2011). Sperm DNA damage or progressive motility: Which one is the better predictor of fertilization in vitro? *Systems Biology in Reproductive Medicine*, 57(3):133–138.

[167] Spindler, R., Rosenhahn, B., Hofmann, N., and Glasmacher, B. (2012). Video analysis of osmotic cell response during cryopreservation. *Cryobiology*, 64(3):250–260.

[168] Steptoe, P. C. and Edwards, R. G. (1978). Birth after the reimplantation of a human embryo. *The Lancet*, 312(8085):366.

[169] Strauss, G. and Hauser, H. (1986). Stabilization of lipid bilayer vesicles by sucrose during freezing. *Proceedings of the National Academy of Sciences of the United States of America*, 83(8):2422–2426.

[170] Swelum, A. A., Mansour, H. A., Elsayed, A. A., and Amer, H. A. (2011). Comparing ethylene glycol with glycerol for cryopreservation of buffalo bull semen in egg-yolk containing extenders. *Theriogenology*, 76(5):833–842.

[171] Thida, M., Chan, K. L., and Eng, H.-l. (2006). An Improved Real-Time Contour Tracking. *Pacific-Rim Symposium on Image and Video Technology (PSIVT)*, pages 702–711.

[172] Thomashow, M. F. (1999). Plant cold acclimation: Freezing tolerance genes and regulatory mechanisms. *Annual Review of Plant Biology*, 50:571–599.

[173] Thurston, L. M., Watson, P. F., and Holt, W. V. (2002). Semen cryopreservation: A genetic explanation for species and individual variation? *Cryo-Letters*, 23(4):255–262.

[174] Tian, Y., Duan, F., Zhou, M., and Wu, Z. (2013). Active contour model combining region and edge information. *Machine Vision and Applications*, 24(1):47–61.

[175] Tomlinson, M. J., Pooley, K., Simpson, T., Newton, T., Hopkisson, J., Jayaprakasan, K., Jayaprakasan, R., Naeem, A., and Pridmore, T. (2010). Validation of a novel computer-assisted sperm analysis (CASA) system using multitarget-tracking algorithms. *Fertility and Sterility*, 93(6):1911–1920.

[176] Toner, M., Cravalho, E. G., and Karel, M. (1990). Thermodynamics and kinetics of intracellular ice formation during freezing of biological cells. *Journal of Applied Physics*, 67(3):1582–1593.

[177] Tsujii, H., Ohta, E., Miah, A. G., Hossain, S., and Salma, U. (2006). Effect of fructose on motility, acrosome reaction and in vitro fertilization capability of boar spermatozoa. *Reproductive Medicine and Biology*, 5(4):255–261.

[178] Tunstall, T., Kock, R., Vahala, J., Diekhans, M., Fiddes, I., Armstrong, J., Paten, B., Ryder, O. A., and Steiner, C. C. (2018). Evaluating recovery potential of the northern white rhinoceros from cryopreserved somatic cells. *Genome Research*, 28(6):780–788.

[179] Uemura, M. and Steponkus, P. L. (1994). A contrast of the plasma membrane lipid composition of oat and rye leaves in relation to freezing tolerance. *Plant Physiology*, 104(2):479–496.

[180] Ugur, M. R., Saber Abdelrahman, A., Evans, H. C., Gilmore, A. A., Hitit, M., Arifiantini, R. I., Purwantara, B., Kaya, A., and Memili, E. (2019). Advances in Cryopreservation of Bull Sperm. *Frontiers in Veterinary Science*, 6(August):1–15.

[181] Ungerfeld, R., Dago, A. L., Rubianes, E., and Forsberg, M. (2004). Response of anestrous ewes to the ram effect after follicular wave synchronization with a single dose of estradiol-17beta. *Reproduction, nutrition, development*, 44(1):89–98.

[182] Vajta, G. and Kuwayama, M. (2006). Improving cryopreservation systems. *Theriogenology*, 65(1):236–244.

[183] Van De Weijer, J. and Gevers, T. (2004). Tensor based feature detection for color images. *Final Program and Proceedings - IS and T/SID Color Imaging Conference*, (May 2014):100–105.

[184] Viana, J. (2019). Statistics of embryo production and transfer in domestic farm animals. *Embryo Technology Newsletter-IETS*, 36(4):1–26.

[185] Vincent, C. and Johnson, M. H. (1992). Cooling, cryoprotectants, and the cytoskeleton of the mammalian oocyte. *Oxford reviews of reproductive biology*, 14:73–100.

[186] Vincent, P., Underwood, S. L., Dolbec, C., Bouchard, N., Kroetsch, T., and Blondin, P. (2014). Bovine Semen Quality Control in Artificial Insemination Centers. *Bovine Reproduction*, pages 685–695.

[187] Wang, X., Al Naib, A., Sun, D. W., and Lonergan, P. (2010). Membrane permeability characteristics of bovine oocytes and development of a step-wise cryoprotectant adding and diluting protocol. *Cryobiology*, 61(1):58–65.

[188] Wang, X., Hua, T.-C., Sun, D.-W., Liu, B., Yang, G., and Cao, Y. (2007). Cryopreservation of tissue-engineered dermal replacement in Me2SO: Toxicity study and effects of concentration and cooling rates on cell viability. *Cryobiology*, 55(1):60–65.

[189] Watson, P. F. (2000). The causes of reduced fertility with cryopreserved semen. *Animal Reproduction Science*, 60-61:481–492.

[190] Wolfe, J. and Bryant, G. (2001). Cellular cryobiology: thermodynamic and mechanical effects. *International Journal of Refrigeration*, 24(5):438–450.

[191] Wolkers, W. F., Oldenhof, H., Tang, F., Han, J., Bigalk, J., and Sieme, H. (2019). Factors Affecting the Membrane Permeability Barrier Function of Cells during Preservation Technologies. *Langmuir*, 35(23):7520–7528.

[192] Woods, E. J., Benson, J. D., Agca, Y., and Critser, J. K. (2004). Fundamental cryobiology of reproductive cells and tissues. *Cryobiology*, 48(2):146–156.

[193] Wowk, B. (2010). Thermodynamic aspects of vitrification. *Cryobiology*, 60(1):11–22.

[194] Wu, P., Yi, J., Zhao, G., Huang, Z., Qiu, B., and Gao, D. (2015). Active contour-based cell segmentation during freezing and its application in cryopreservation. *IEEE Transactions on Biomedical Engineering*, 62(1):284–295.

[195] Xu, C., Yezzi A., J., and Prince, J. L. (2000). On the relationship between parametric and geometric active contours. *Conference Record of the Asilomar Conference on Signals, Systems and Computers*, 1(October):483–489.

[196] Yang, H., Carmichael, C., Varga, Z. M., and Tiersch, T. R. (2007). Development of a simplified and standardized protocol with potential for high-throughput for sperm cryopreservation in zebrafish Danio rerio. *Theriogenology*, 68(2):128–136.

[197] Yeste, M., Flores, E., Estrada, E., Bonet, S., Rigau, T., and Rodríguez-Gil, J. E. (2013). Reduced glutathione and procaine hydrochloride protect the nucleoprotein structure of boar spermatozoa during freeze-thawing by stabilising disulfide bonds. *Reproduction, Fertility and Development*, 25(7):1036–1050.

[198] Yin, F., Mao, H., and Hua, L. (2011). A hybrid of back propagation neural network and genetic algorithm for optimization of injection molding process parameters. *Materials and Design*, 32(6):3457–3464.

[199] Zeron, Y., Pearl, M., Borochov, A., and Arav, A. (1999). Kinetic and Temporal Factors Influence Chilling Injury to Germinal Vesicle and Mature Bovine Oocytes. *Cryobiology*, 38(1):35–42.

[200] Zhang, J. M., Sheng, Y., Cao, Y. Z., Wang, H. Y., and Chen, Z. J. (2011). Effects of cooling rates and ice-seeding temperatures on the cryopreservation of whole ovaries. *Journal of Assisted Reproduction and Genetics*, 28(7):627–633.

[201] Zhao, G. and Fu, J. (2017). Microfluidics for cryopreservation. *Biotechnology advances*, 35(2):323–336.

[202] Zhu, Z., Fan, X., Pan, Y., Lu, Y., and Zeng, W. (2017). Trehalose improves rabbit sperm quality during cryopreservation. *Cryobiology*, 75:45–51.

[203] Zorgniotti, A. W. and AW, Z. (1975). The spermatozoa count. A short history.